



저작자표시-비영리-변경금지 2.0 대한민국

이용자는 아래의 조건을 따르는 경우에 한하여 자유롭게

- 이 저작물을 복제, 배포, 전송, 전시, 공연 및 방송할 수 있습니다.

다음과 같은 조건을 따라야 합니다:



저작자표시. 귀하는 원저작자를 표시하여야 합니다.



비영리. 귀하는 이 저작물을 영리 목적으로 이용할 수 없습니다.



변경금지. 귀하는 이 저작물을 개작, 변형 또는 가공할 수 없습니다.

- 귀하는, 이 저작물의 재이용이나 배포의 경우, 이 저작물에 적용된 이용허락조건을 명확하게 나타내어야 합니다.
- 저작권자로부터 별도의 허가를 받으면 이러한 조건들은 적용되지 않습니다.

저작권법에 따른 이용자의 권리는 위의 내용에 의하여 영향을 받지 않습니다.

이것은 [이용허락규약\(Legal Code\)](#)을 이해하기 쉽게 요약한 것입니다.

[Disclaimer](#)

공학석사학위논문

**Design of Least-Square Switching Function
for Accurate and Efficient Gradient
Estimation on Unstructured Grid**

비정렬격자에서 정확하고 효율적인 구배 계산을
위한 최소제곱법 스위칭 함수 설계

2019 년 2 월

서울대학교 대학원

기계항공공학부

서 승 표

Design of Least-Square Switching Function for Accurate and Efficient Gradient Estimation on Unstructured Grid

비정렬격자에서 정확하고 효율적인 구배 계산을
위한 최소제곱법 스위칭 함수 설계

지도교수 김 종 암




이 논문을 공학석사 학위논문으로 제출함

2019 년 2 월

서울대학교 대학원
기계항공공학부
서 승 표

서승표의 공학석사 학위논문을 인준함

2019 년 2 월

위원장	<u>김 규 흥</u>	
부위원장	<u>김 공 안</u>	
위원	<u>이 관 중</u>	

Abstract

Design of Least-Square Switching Function for Accurate and Efficient Gradient Estimation on Unstructured Grid

Seungpyo Seo

Department of Mechanical and Aerospace Engineering

The Graduate School

Seoul National University

The present work proposes accurate and efficient gradient estimation on unstructured grid by designing a switching function between two Least-Square methods. Through various test cases, it is shown that gradient by Green-Gauss theorem, one of the most widely preferred gradient estimation on unstructured grid, is inherently inconsistent, and gradient by Least-Square methods show higher gradient accuracy on viscous boundary layer and general grid compared to Green-Gauss approach.

Regarding the observation, switching between two Least-Square methods, relatively efficient compact weighted Least-Square method and accurate extended weighted Least-

Square method, is pursued. Since condition number of the Least-Square matrix can be calculated from the geometric information of the given grid, and shows correlation with the gradient error, it is chosen as the switching criterion. To implement on general grid, the condition number is analyzed and formulated as the function of number of stencils and angle between stencil vectors using trigonometric relations. Then, it is confirmed that average condition number of extended weighted Least-Square method is suitable switching criterion value.

The switching mechanism is demonstrated through two and three-dimensional simple cases. Finally, comparison of gradient accuracy and computational cost of three Least - Square methods are addressed on two-dimensional airfoil, three-dimensional wing-body and modern fighter configuration to show the excellence of SWLSQ.

Keywords: Gradient, Gradient estimation method, Least-Square method, Switching Function, Condition number, Green-Gauss theorem, Unstructured grid

Student Number: 2017-29318

Contents

	Page
Abstract	i
Contents	iii
List of Tables	vi
List of Figures	vii
Chapter 1 Introduction	1
1.1 Background.....	1
1.2 Research Objective.....	2
Chapter 2 Numerical Methods	4
2.1 Governing Equations.....	4
2.2 Gradient Estimation Methods on Unstructured Grid.....	7
2.2.1 Least-Square Method.....	7
2.2.1.1 The Method of Normal Equations.....	10
2.2.1.2 Weighting Function.....	12
2.2.1.3 QR Factorization.....	13
2.2.2 Green-Gauss Theorem.....	15
2.2.2.1 Simple Averaging.....	16
2.2.2.2 Node Averaging.....	17
Chapter 3 Analysis on Preceding Approaches	19
3.1 Numerical Test.....	19
3.1.1 Grid Type.....	19

3.1.2 Test Function.....	22
3.2 Observation.....	24
3.2.1 Quadrilateral grid with test functions.....	24
3.2.2 Results by Green-Gauss type methods.....	28
3.2.3 Results by Least-Square type methods.....	29
Chapter 4 Least-Square Method Switching Function.....	31
4.1 Motivation.....	31
4.2 Switching Criterion.....	32
4.2.1 Conventional Grid Quality Criterion.....	32
4.2.2 Condition Number of Least-Square Matrix.....	34
4.2.3 Condition Number Calculation Method.....	38
4.2.3.1 Quadratic Formula.....	38
4.2.3.2 Power Method.....	39
4.3 Switching Least-Square Method.....	41
4.3.1 Behavior of Condition Number of CWLSQ and EWLSQ.....	41
4.3.2 Switching Procedure.....	44
4.4 Simple Demonstration.....	46
4.4.1 Two-Dimensional Randomly Diagonalized Triangular Grid.....	46
4.4.2 Three-Dimensional Random tetrahedral Grid.....	48
Chapter 5 Application.....	49
5.1 Two-Dimensional NACA0012 Airfoil.....	49
5.2 Three-Dimensional Wing-Body Configuration.....	51
5.2.1 Test Function.....	51

5.2.2 Flow Simulation.....	52
5.3 Three-Dimensional Modern Fighter.....	55
5.3.1 Test Function.....	55
5.3.2 Flow Simulation.....	57
Chapter 6 Conclusion.....	59
References.....	61
국문초록.....	64

List of Tables

	Page
Table 3.1 Notation of grid and test function types.....	23
Table 5.1 Summary of information of the flow simulation over NACA0012.....	49
Table 5.2 Summary of information of the flow simulation over the CRM.....	53
Table 5.3 Aerodynamic coefficients and computation time of two LSQ methods.....	53
Table 5.4 Summary of information of the flow simulation over the fighter.....	56
Table 5.5 The number and ratio of switched cells.....	57
Table 5.6 Aerodynamic coefficients error and computation time of two LSQ method...57	

List of Figure

	Page
Figure 1.1 Solution reconstruction stage in MUSCL scheme.....	1
Figure 1.2 The region where gradient degradation occurs around the aircraft.....	3
Figure 1.3 Poor gradient accuracy around the complex geometry of the aircraft.....	3
Figure 2.1 Stencil configuration of CWLSQ and EWLSQ.....	9
Figure 2.2 Schematic of the method of normal equations for Least-Square problem.....	10
Figure 2.3 Stencil configuration of GGSA and GGNA.....	18
Figure 3.1 Five types of grid structure for numerical test.....	21
Figure 3.2 Comparison of results from quadrilateral grid.....	24
Figure 3.3 One-dimensional stencil configuration with non-uniform spacing.....	25
Figure 3.4 Contours of gradient error by GGSA and GGNA.....	28
Figure 3.5 Contours of gradient error by CWLSQ and EWLSQ.....	30
Figure 4.1 Gradient error with respect to conventional grid quality criteria.....	33
Figure 4.2 Comparison of two LSQ methods for condition and gradient error.....	35
Figure 4.3 Comparison of CWLSQ and EWLSQ result from U-Q and R-Q test case.....	36
Figure 4.4 Alternative expression by using trigonometric functions and identities.....	42
Figure 4.5 Condition number calculation example of CWLSQ and EWLSQ.....	44
Figure 4.6 Overall procedure of SWLSQ.....	45
Figure 4.7 Comparison of three LSQ methods on R-Q test case.....	47
Figure 4.8 Comparison of three LSQ methods on three-dimensional test case.....	48

Figure 5.1 Comparison of three LSQ methods on two-dimensional NACA0012.....	50
Figure 5.2 Comparison of three LSQ methods on the CRM.....	52
Figure 5.3 Pressure contour of the CRM.....	53
Figure 5.4 Comparison of three Least-Square methods.....	55
Figure 5.5 Comparison of second-gradient error of three Least-Square methods.....	55
Figure 5.6 Comparison of second-gradient error of the two Least-Square methods.....	57

Chapter 1

Introduction

1.1 Background

In modern compressible flow CFD code, Monotonic Upwind Scheme for Conservation Laws (MUSCL) type schemes with second-order accurate spatial discretization are widely used in Finite Volume Method (FVM) cell-centered frame. In the solution reconstruction stage of MUSCL type schemes [1], as well as for calculation of viscous flux and turbulent source term, gradient estimation plays an important role for the accuracy and robustness of the dependent variable.

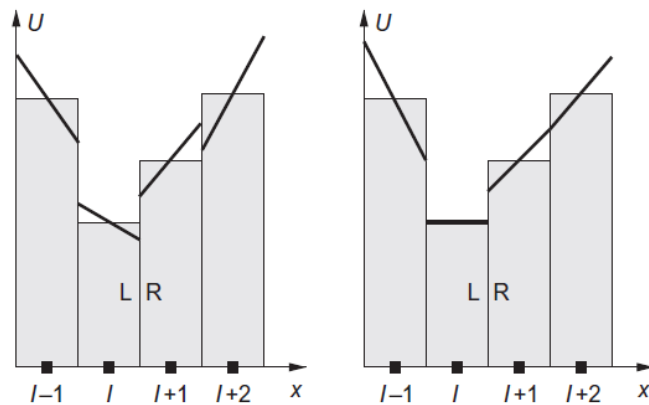


Figure 1.1 Solution reconstruction stage in MUSCL scheme with and without a limiter

Unlike the structured grid, unstructured grid does not have an ordered cell-connectivity that classic ways of estimating a gradient used in structured grid are not applicable. On unstructured grid, gradient estimation by Green-Gauss theorem (GG) and Least-Square method (LSQ) are widely preferred approaches, but no optimal solution exists in terms of accuracy, robustness and efficiency. Mavriplis [2] indicated that gradient accuracy of non-weighting, compact LSQ can be poor on high aspect ratio cell with surface curvature. Diskin *et al.* [3] and Correa *et al.* [4] compared existing gradient estimation methods on various regular and irregular meshes. Meanwhile, Shima *et al.* [5] tried to combine the advantages of two gradient estimation methods, gradient by Green Gauss theorem and gradient by Least-Square methods.

On the other hands, it was found that bad grid quality around the complex geometry of the aircraft, especially at the small space between the control surface and the nozzle as presented in Fig. 1.2 and Fig. 1.3, deteriorates the gradient accuracy. This gradient accuracy degradation brings about the numerical oscillation at the region, eventually leading to the computation failure. Full configuration of the aircraft is not presented here for confidentiality policy.

The objective of this work to propose accurate and efficient gradient estimation method on arbitrary unstructured grid. More specifically, we propose a switching criterion that can be applied to conversion between CWLSQ and EWLSQ, by analyzing it qualitatively and quantitatively.

This thesis is organized in the following order. To begin with, chapter 2 introduces the numerical methods covered in this work, including basic information of the governing

equations and existing gradient estimation methods. Next, chapter 3 outlines analysis made on preceding gradient estimation approaches. Chapter 4 deals with process of how the switching criterion is established, forming the Switching Least-Square method. Chapter 5 compares the SWLSQ with two LSQ methods, CWLSQ and EWLSQ, on two and three-dimensional flow problems to show the excellence of SWLSQ. Lastly, conclusions and necessity of future work are addressed in Chapter 6.

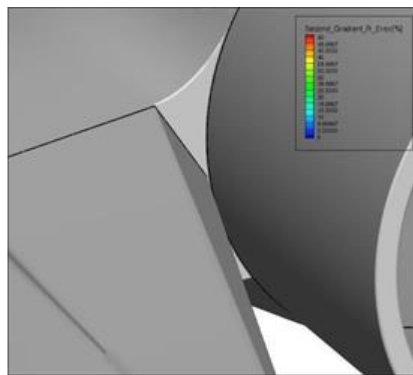


Figure 1.2 The region where gradient deterioration occurs around the aircraft

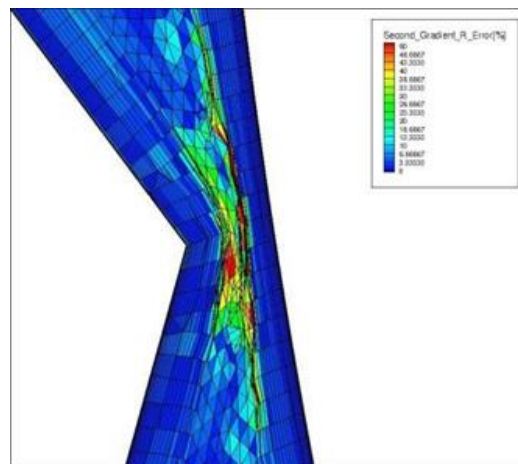


Figure 1.3 Poor gradient accuracy around the complex geometry of the aircraft

Chapter 2

Numerical Methods

2.1 Governing Equations

The governing equations are three-dimensional Navier-Stokes equations, which can be written in an integral form as follows for control volume Ω and surrounding control surface S

$$\frac{\partial}{\partial t} \int_{\Omega} \vec{W} d\Omega + \oint_{\partial\Omega} (\vec{F}_c - \vec{F}_v) dS = \int_{\Omega} \vec{Q} d\Omega. \quad (2.1)$$

\vec{W} stands for a vector of the conservative variable consisting of five components

$$\vec{W} = \begin{bmatrix} \rho \\ \rho u \\ \rho v \\ \rho w \\ \rho E \end{bmatrix} \quad (2.2)$$

where ρ , u , v and w are density, x-direction velocity, y-direction velocity, z-direction velocity respectively. Furthermore, E is total energy per unit mass of a fluid obtained from summation of internal energy per unit mass, e , and its kinetic energy per unit mass $|v|^2/2$, i.e.,

$$E = e + \frac{|v|^2}{2} = e + \frac{u^2 + v^2 + w^2}{2}. \quad (2.3)$$

In addition, \vec{F}_c is the vector of convective fluxes which describes the contribution of flow quantities going through the control surface with the velocity \vec{v}

$$\vec{F}_c = \begin{bmatrix} \rho V \\ \rho u V + n_x p \\ \rho v V + n_y p \\ \rho w V + \\ \rho H V \end{bmatrix} \quad (2.4)$$

in which V is the velocity normal to the surface element dS , or contravariant velocity, with definition

$$V \equiv \vec{v} \cdot \mathbf{n} = un_x + vn_y + wn_z. \quad (2.5)$$

\vec{F}_v is the vector of viscous fluxes

$$\vec{F}_v = \begin{bmatrix} 0 \\ n_x \tau_{xx} + n_y \tau_{xy} + n_z \tau_{xz} \\ n_x \tau_{yx} + n_y \tau_{yy} + n_z \tau_{yz} \\ n_x \tau_{zx} + n_y \tau_{zy} + n_z \tau_{zz} \\ n_x \Theta_x + n_y \Theta_y + n_z \Theta_z \end{bmatrix} \quad (2.6)$$

where

$$\begin{aligned} \Theta_x &= u\tau_{xx} + v\tau_{xy} + w\tau_{xz} + k \frac{\partial T}{\partial x}, \\ \Theta_y &= u\tau_{yx} + v\tau_{yy} + w\tau_{yz} + k \frac{\partial T}{\partial y}, \\ \Theta_z &= u\tau_{zx} + v\tau_{zy} + w\tau_{zz} + k \frac{\partial T}{\partial z} \end{aligned} \quad (2.7)$$

are terms expressing the work of the viscous stress and of the heat conduction in the fluid respectively. τ_{ij} denotes a stress component of the viscous stress tensor, originated from the friction between the fluid and the surface of an element. Under the assumption of Newtonian fluid, τ_{ij} is thought to be proportional to the velocity gradient

$$\begin{aligned} \tau_{xx} &= \lambda \left(\frac{\partial u}{\partial x} + \frac{\partial v}{\partial y} + \frac{\partial w}{\partial z} \right) + 2\mu \frac{\partial u}{\partial x}, \\ \tau_{yy} &= \lambda \left(\frac{\partial u}{\partial x} + \frac{\partial v}{\partial y} + \frac{\partial w}{\partial z} \right) + 2\mu \frac{\partial v}{\partial y}, \end{aligned} \quad (2.8)$$

$$\tau_{zz} = \lambda \left(\frac{\partial u}{\partial x} + \frac{\partial v}{\partial y} + \frac{\partial w}{\partial z} \right) + 2\mu \frac{\partial w}{\partial z},$$

$$\tau_{xy} = \tau_{yx} = \mu \left(\frac{\partial u}{\partial y} + \frac{\partial v}{\partial x} \right),$$

$$\tau_{xz} = \tau_{zx} = \mu \left(\frac{\partial u}{\partial z} + \frac{\partial w}{\partial x} \right),$$

$$\tau_{yz} = \tau_{zy} = \mu \left(\frac{\partial v}{\partial z} + \frac{\partial w}{\partial y} \right)$$

where λ is referred to as the second viscosity coefficient, and μ represents the dynamic viscosity coefficient. Lastly, \vec{Q} in Eq. (2.1) is the source term with the components

$$\vec{Q} = \begin{bmatrix} 0 \\ \rho f_{e,x} \\ \rho f_{e,y} \\ \rho f_{e,z} \\ \rho \vec{f}_e \cdot \vec{v} + q_h \end{bmatrix} \quad (2.9)$$

with $\rho f_{e,i}$ accounting for the effect of body forces, such as gravitational force, and q_h denoting time rate of heat transfer.

2.2 Gradient Estimation Methods on Unstructured Grids

2.2.1 Least-Square Method

Least-Square method is a general approach to find optimal solution for overdetermined system by minimizing the sum of the square of the residuals. Residual means the difference between the fitted value and observed data. In overdetermined system, the number of equations is greater than the number of unknowns so that no exact solution exists, except for the case where one equation is linear combination of others.

As for FVM cell-centered schemes, the gradient as well as other flow quantities are assumed to be located at centroid of each control volume, which is identical to a grid cell. Herewith, Least-Square formulation is derived from the Taylor series approximation with respect to the cell where the gradient is to be evaluated. Taylor series approximation of the cell i to the neighboring cell j (or stencil) can be expressed as follows

$$\phi_j = \phi_i + \nabla\phi_i \cdot \vec{d}_{ij} + O(h^2) \quad (2.10)$$

$$\nabla\phi_i \cdot \vec{d}_{ij} = \Delta\phi_{ij} + O(h^2) \quad (2.11)$$

where ϕ is flow variable at the cell-center, and $\vec{d}_{ij} = \vec{d}_j - \vec{d}_i$ is the distance vector from the cell i to the stencil j . Further, $O(h^2)$ denotes second-order truncation error, which is usually neglected in Least-Square formulation, and h is a characteristic grid spacing. Writing down Eq. (2.11) to all neighboring cell j , we obtain following overdetermined system of linear equations

$$\begin{bmatrix} \Delta x_{i1} & \Delta y_{i1} & \Delta z_{i1} \\ \Delta x_{i2} & \Delta y_{i2} & \Delta z_{i2} \\ \vdots & \vdots & \vdots \\ \Delta x_{iN} & \Delta y_{iN} & \Delta z_{iN} \end{bmatrix} \begin{bmatrix} \left(\frac{\partial \phi}{\partial x}\right)_i \\ \left(\frac{\partial \phi}{\partial y}\right)_i \\ \left(\frac{\partial \phi}{\partial z}\right)_i \end{bmatrix} = \begin{bmatrix} \Delta \phi_{i1} \\ \Delta \phi_{i2} \\ \vdots \\ \Delta \phi_{iN} \end{bmatrix} \quad (2.13)$$

with $\Delta(\cdot)_{ij} = (\cdot)_j - (\cdot)_i$, and N is the number of stencils used for estimation of gradient.

In abbreviation, Eq. (2.13) is expressed as

$$A\vec{x} = \vec{b}. \quad (2.14)$$

On the other hand, choices of stencil for the Least-Square method have been studied by many researchers [3,6,7,8]. In this paper, two types of scope of stencil will be mainly dealt with, compact stencil and extended stencil. When we use neighboring cells, who are sharing a cell face with the target cell, where the gradient is estimated, these neighboring stencils are called compact stencil, leading to Compact stencil Weighted Least-Square method (CWLSQ). Extended stencil, covering larger range than compact stencil, means neighboring cells who are sharing a node with the target cell, also referred to as Extended stencil Weighted Least-Square method (EWLSQ). Fig. 2.1 illustrates the stencil configuration of Least-Square method using compact and extended stencil.

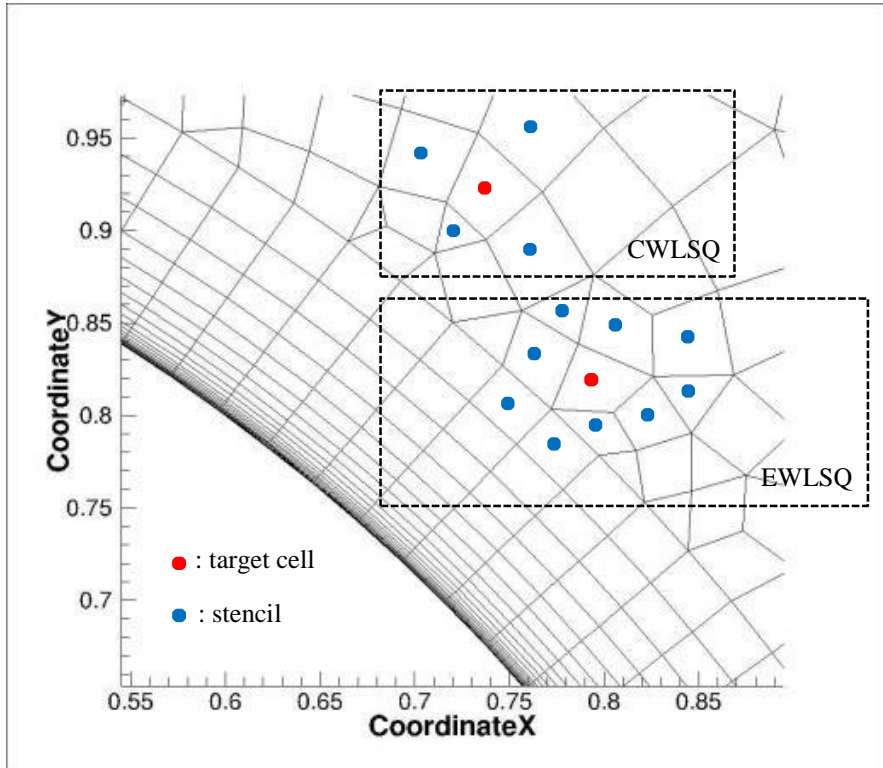


Figure 2.1 Stencil configuration of CWLSQ and EWLSQ

2.2.1.1 The Method of Normal Equations

A generally adopted approach to solve Least-Square problem is the method of normal equations. In mathematical sense, overdetermined system, where no solution x exists satisfying Eq. (2.14), implies \vec{b} is not in the column space of A as described in Fig. 2.2.

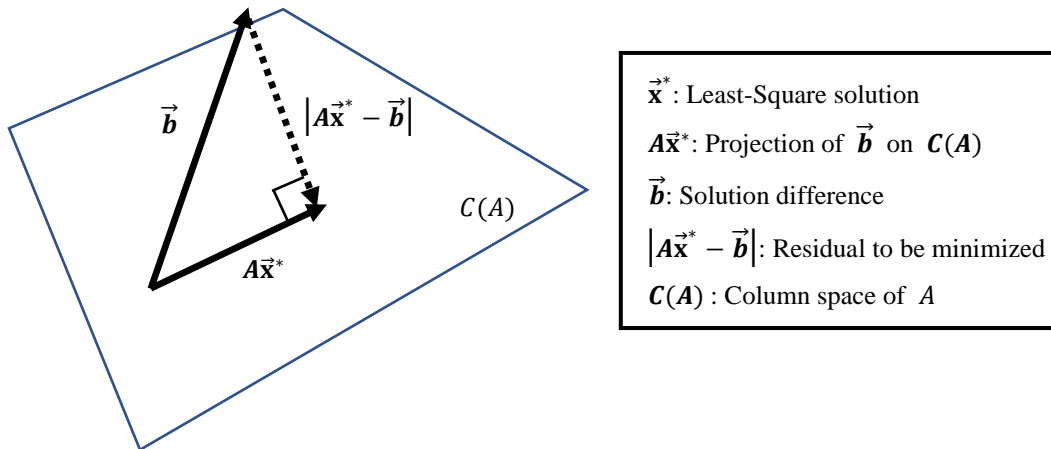


Figure 2.2 Schematic of the method of normal equations for Least-Square problem

The optimal Least-Square solution \vec{x}^* that minimizes the residual is the projection of the \vec{b} to the column space of A , $C(A)$. Meanwhile, from the relation of $C(A)$ to the null space

$$C(A)^\perp = N(A^T) \quad (2.15)$$

, and since $A\vec{x}^* - \vec{b}$ is an element of orthogonal complement of column space of A

$$(A\vec{x}^* - \vec{b}) \in C(A)^\perp, \quad (2.16)$$

following normal equation can be derived

$$A^T(A\vec{x}^* - \vec{b}) = 0. \quad (2.17)$$

Expanding and rearranging the normal equation, we obtain

$$A^T A\vec{x}^* - A^T \vec{b} = 0 \quad (2.18)$$

$$A^T A\vec{x}^* = A^T \vec{b} \quad (2.19)$$

, or in matrix form

$$\begin{bmatrix} \sum_j^N (\Delta x_j)^2 & \sum_j^N \Delta x_j \Delta y_j & \sum_j^N \Delta x_j \Delta z_j \\ \sum_j^N \Delta x_j \Delta y_j & \sum_j^N (\Delta y_j)^2 & \sum_j^N \Delta y_j \Delta z_j \\ \sum_j^N \Delta x_j \Delta z_j & \sum_j^N \Delta y_j \Delta z_j & \sum_j^N (\Delta z_j)^2 \end{bmatrix} \begin{bmatrix} \left(\frac{\partial \phi}{\partial x}\right)_i^* \\ \left(\frac{\partial \phi}{\partial y}\right)_i^* \\ \left(\frac{\partial \phi}{\partial z}\right)_i^* \end{bmatrix} = \begin{bmatrix} \sum_j^N \Delta x_j \Delta \phi_{ij} \\ \sum_j^N \Delta y_j \Delta \phi_{ij} \\ \sum_j^N \Delta z_j \Delta \phi_{ij} \end{bmatrix}. \quad (2.20)$$

Finally, taking the inverse of $(A^T A)$, \vec{x}^* is expressed as follows

$$\vec{x}^* = (A^T A)^{-1} A^T \vec{b}. \quad (2.21)$$

2.2.1.2 Weighting Function

Least-Square method without proper weighting function may present bad gradient accuracy at a cell with high aspect ratio on surface curvature [2]. After weighting function is applied to each stencil, Eq. (2.20) can be cast into the following form

$$\begin{bmatrix} \sum_j^N w_j (\Delta x_j)^2 & \sum_j^N w_j \Delta x_j \Delta y_j & \sum_j^N w_j \Delta x_j \Delta z_j \\ \sum_j^N w_j \Delta x_j \Delta y_j & \sum_j^N w_j (\Delta y_j)^2 & \sum_j^N w_j \Delta y_j \Delta z_j \\ \sum_j^N w_j \Delta x_j \Delta z_j & \sum_j^N w_j \Delta y_j \Delta z_j & \sum_j^N w_j (\Delta z_j)^2 \end{bmatrix} \begin{bmatrix} \left(\frac{\partial \phi}{\partial x}\right)_i^* \\ \left(\frac{\partial \phi}{\partial y}\right)_i^* \\ \left(\frac{\partial \phi}{\partial z}\right)_i^* \end{bmatrix} = \begin{bmatrix} \sum_j^N w_j \Delta x_j \Delta \phi_{ij} \\ \sum_j^N w_j \Delta y_j \Delta \phi_{ij} \\ \sum_j^N w_j \Delta z_j \Delta \phi_{ij} \end{bmatrix} \quad (2.22)$$

or in abbreviation

$$\bar{A} \vec{x}^* = \vec{b}. \quad (2.23)$$

A typical treatment of weighting function is taking inverse square of distance between two points, the target cell and the stencil

$$w_j = 1/|\vec{d}_{ij}|^2 \quad (2.24)$$

where \vec{d}_{ij} is same as in Eq. (2.11). In this study, this approach will be used as the basic weighting function. Meanwhile, alternative choices of weighting function have been analyzed by other research [5,10].

2.2.1.3 QR Factorization

To solve the linear system of equations Eq. (2.23), a matrix inversion is essential. However, it is known that a cell with highly stretched cell is prone to become an ill-conditioned system, which subsequently brings about another remedy, QR Factorization [11,12].

Following is the description of QR factorization procedure explained in the reference [13]. By using the Gram-Schmidt process, the Least-Square the matrix $\bar{A} = [\vec{a}_1, \vec{a}_2, \vec{a}_3]$ from Eq. (2.23) can be decomposed into orthogonal matrix $Q = [\vec{q}_1, \vec{q}_2, \vec{q}_3]$ and upper triangular matrix R , whose component is denoted as r_{ij} ,

$$(QR)\vec{x}^* = \vec{b} \quad (2.25)$$

where

$$\begin{aligned} \vec{q}_1 &= \frac{1}{r_{11}} \vec{a}_1, \\ \vec{q}_2 &= \frac{1}{r_{22}} \left(\vec{a}_2 - \frac{r_{12}}{r_{11}} \vec{a}_1 \right), \\ \vec{q}_3 &= \frac{1}{r_{33}} \left[\vec{a}_3 - \frac{r_{23}}{r_{22}} \vec{a}_2 - \left(\frac{r_{13}}{r_{11}} - \frac{r_{12} r_{23}}{r_{11} r_{22}} \right) \vec{a}_1 \right]. \end{aligned} \quad (2.26)$$

$$r_{11} = \sqrt{\sum_{j=1}^{N_A} (\Delta x_{ij})^2}, \quad (2.27)$$

$$r_{12} = \frac{1}{r_{11}} \sum_{j=1}^{N_A} \Delta x_{ij} \Delta y_{ij},$$

$$r_{22} = \sqrt{\sum_{j=1}^{N_A} (\Delta y_{ij})^2 - r_{12}^2},$$

$$r_{13} = \frac{1}{r_{11}} \sum_{j=1}^{N_A} \Delta x_{ij} \Delta z_{ij},$$

$$r_{23} = \frac{1}{r_{22}} \left(\sum_{j=1}^{N_A} \Delta y_{ij} \Delta z_{ij} - \frac{r_{12}}{r_{11}} \sum_{j=1}^{N_A} \Delta x_{ij} \Delta z_{ij} \right),$$

$$r_{33} = \sqrt{\sum_{j=1}^{N_A} (\Delta z_{ij})^2 - (r_{13}^2 + r_{23}^2)}.$$

Here, weighting function w_j is set to unity for convenience. Since Q is an orthogonal matrix, transpose of Q is same as inverse of Q , i.e.

$$Q^T = Q^{-1} \quad (2.28)$$

Therefore, substituting the above relation to solve the Eq. (2.25) for \vec{x}^* ,

$$\vec{x}^* = R^{-1} Q^T \vec{b}. \quad (2.29)$$

2.2.2 Green-Gauss Theorem

The gradient estimation by Green-Gauss theorem, or divergence theorem, is derived from the relation that volume integral of first derivative of the flow variable $\nabla\phi$ is equal to the surface integral of the flow variable ϕ at the given location

$$\iiint_V \nabla\phi dV = \oiint_A \phi \vec{n} dA \quad (2.30)$$

where V and A denote the control volume and the surrounding surface respectively. Furthermore, dV and dA are infinitesimally small volume and surface element respectively with unit normal vector \vec{n} pointing outward of the cell. As for cell-centered FVM, assuming constant flow variable within the control volume, Eq. (2.30) can be rewritten as follows

$$V\nabla\phi = \oiint_A \phi \vec{n} dA \quad (2.31)$$

with V indicating the volume of the grid cell. In the same context, surface integral on the right-hand side of Eq. (2.31) can be approximated by sum of the flow variable crossing the faces of the surrounding surface, called spatial discretization,

$$V\nabla\phi = \sum_{k=1}^N \bar{\phi}_k \vec{n}_k A_k. \quad (2.32)$$

In the above Eq. (2.32), N refers to the number of faces of the control volume, and $\bar{\phi}_k$ is the average flow variable assumed to be placed at the midpoint of the k -th face. In addition, \vec{n}_k and A_k are unit normal vector and face area of the k -th face respectively. Denoting a

specific cell using a subscript i and dividing both sides of the Eq. (2.32) by V , we can express the gradient by the Green-Gauss theorem as follows

$$\nabla\phi_i = \frac{1}{V} \sum_{k=1}^N \bar{\phi}_k \vec{n}_k A_k. \quad (2.33)$$

To estimate the gradient by using Eq. (2.33), one should identify $\bar{\phi}_f$, an average flow quantity at the midpoint of the k -th face. However, an exact value of $\bar{\phi}_k$ cannot be obtained directly, and thus an approximation for $\bar{\phi}_k$ is inevitable. In the following sub-chapters, two ways of approximating the cell-interface value are dealt with.

2.2.2.1 Simple Averaging

A common way to interpolate the cell-interface value is simply taking the mean value from the left and right quantity of the face, because it is straightforward and requires little effort for implementation

$$\bar{\phi}_f = \frac{1}{2}(\phi_l + \phi_r) \quad (2.34)$$

where ϕ_l and ϕ_r are values from the left and right side of the interface respectively.

For these reasons, gradient by Green-Gauss theorem with simple averaging (GGSA) is usually taken as the basic approach in other research where there is no relevant statement about the approximation of cell-interface value. Despite of advantages regarding simplicity, basically, this approach is not linear-exact, indicating that this method alone cannot restore

the gradient value of the given function even if the function used is linear. More details will be handled in next chapters.

2.2.2.2 Node Averaging

Another way of interpolating the cell-interface value is averaging the quantities of nodes consisting the face. The gradient by Green-Gauss theorem with node averaging (GGNA) are taken into two steps: flow quantities encompassing a node are averaged to obtain the node value, with or without inverse distance weighting, and the calculated node values are averaged to interpolate the cell-interface value.

$$\text{Step1:} \quad \bar{\phi}_n = \frac{\sum_{j=1}^N \bar{\phi}_i / |\vec{d}_j|}{\sum_{j=1}^N 1/|\vec{d}_j|}. \quad (2.35)$$

$$\text{Step2:} \quad \bar{\phi}_f = \frac{1}{\text{number of nodes}} (\bar{\phi}_1 + \bar{\phi}_2 + \dots + \bar{\phi}_n) \quad (2.36)$$

Here $\bar{\phi}_n$ indicates the node value, and \vec{d}_j refers to a distance from the node to adjacent cell-center. Although GGNA often gives more accurate gradient estimation than GGSA, this methodology also is not free from linear-exactness problem; further explanation of this property will be dealt in next chapter together with GGSA. Stencil topology of GGSA and GGNA are illustrated in Fig 2.3.

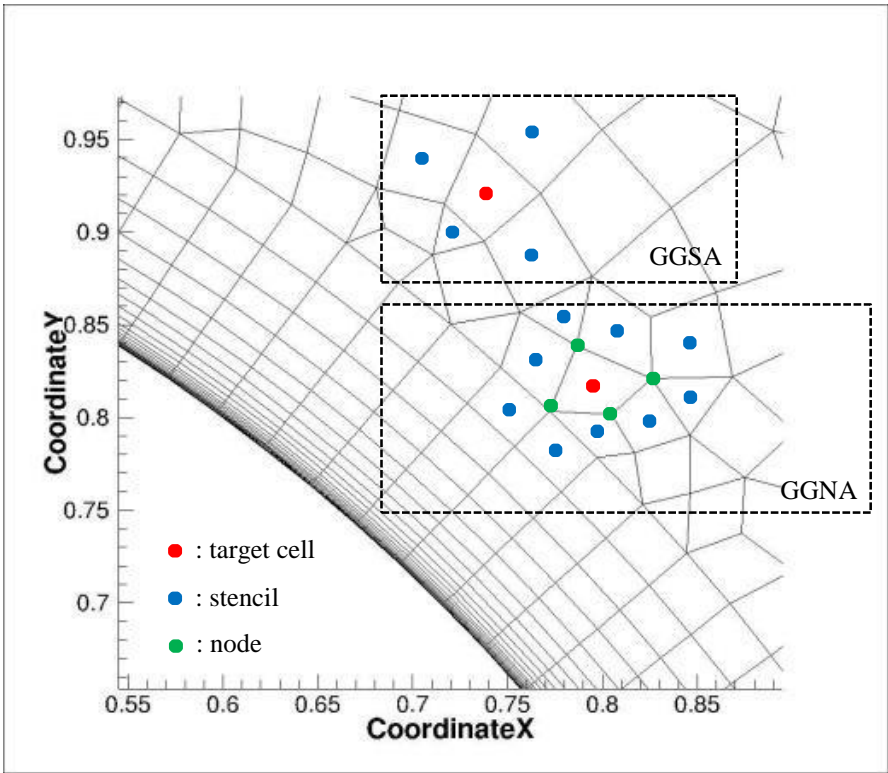


Figure 2.3 Stencil configuration of GGSA and GGNA

Chapter 3

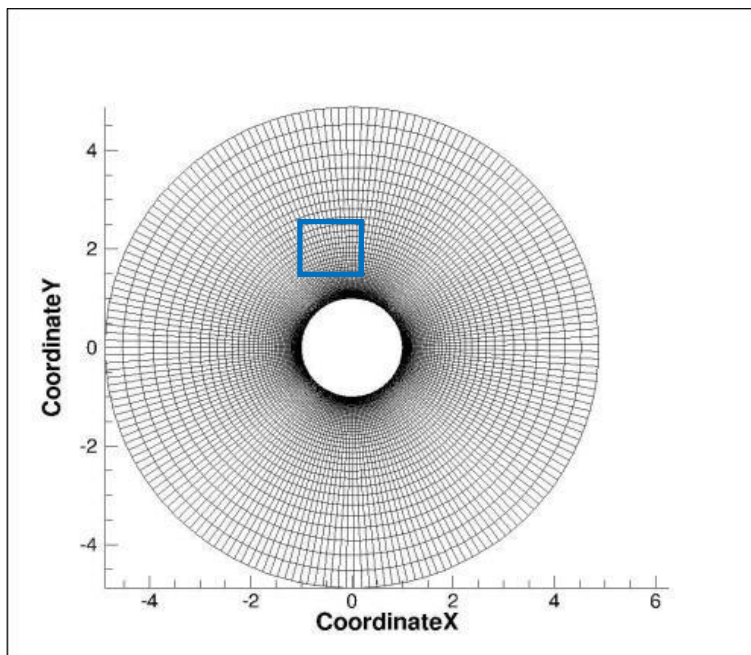
Analysis on Preceding Approaches

3.1 Numerical Test

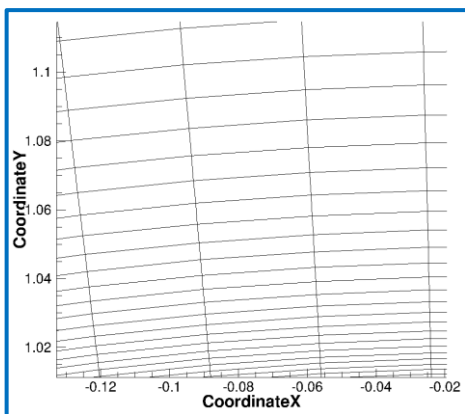
In this chapter, the existing gradient estimation methods, dealt with in previous chapter, are going to be analyzed on various grid types together with two test functions.

3.1.1 Grid Type

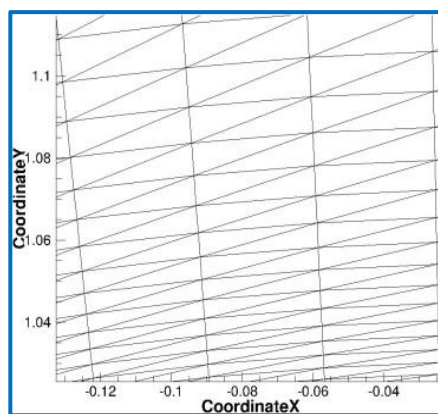
For numerical test, five types of grids are examined: quadrilateral grid, uniformly diagonalized triangular grid, randomly diagonalized triangular grid, mixed grid around a circular cylinder and unstructured NACA0012 airfoil grid. Basically, triangular and mixed grids are variants of the quadrilateral grid in a sense that they were obtained by manipulation of the grid around the cylinder. Meanwhile, all grid types include cells with high aspect ratio near the wall, which are usually observed at viscous boundary layer. Since these cells are known to degrade gradient accuracy estimated by Least-Square methods, this region has been the major concern of some work [8,14]. Fig. 3.1 illustrates five grid structures where as for the triangular and mixed grids, only magnified grid images are posted for brevity



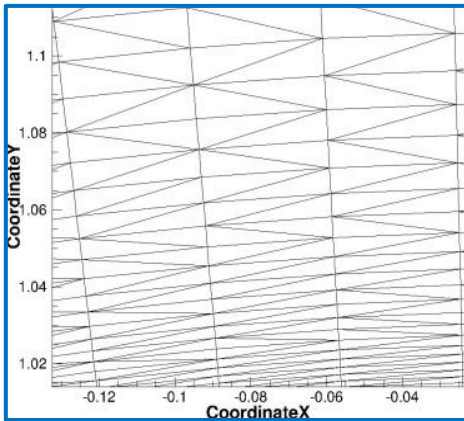
(a) Quadrilateral grid around a circular cylinder



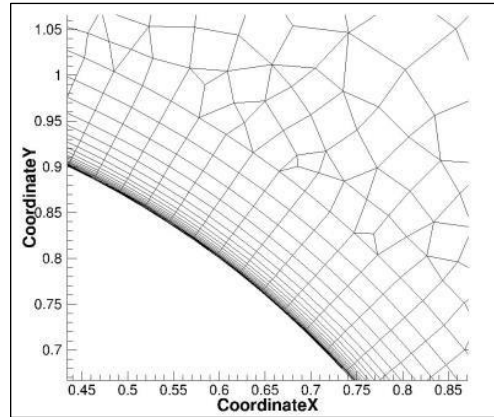
(b) quadrilateral grid (magnified)



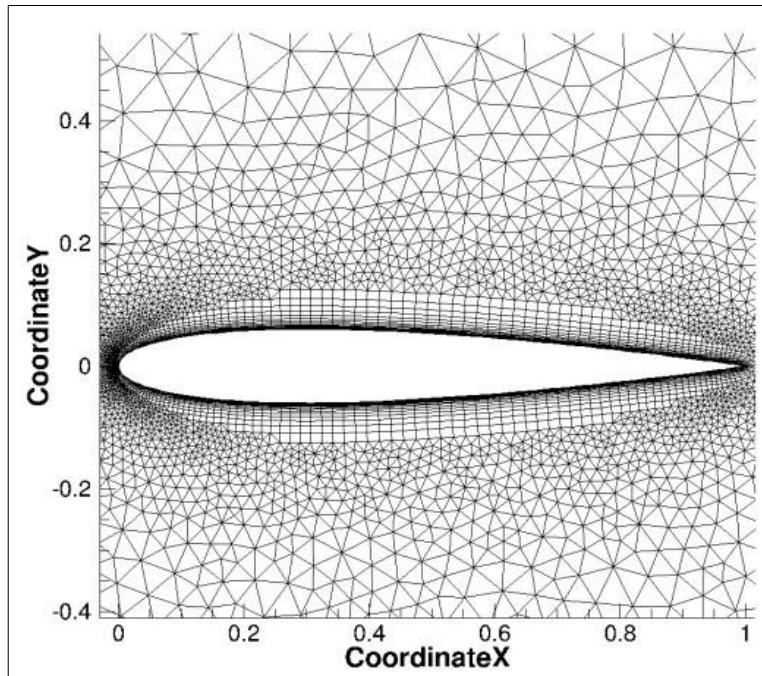
(c) uniformly diagonalized triangular grid (magnified)



(d) randomly diagonalized triangular grid (magnified)



(e) mixed grid around a circular cylinder



(f) Unstructured NACA0012 grid

Figure 3.1 Five types of grid structure for numerical test

3.1.2 Test Function

Evaluating the gradient accuracy necessitates the test function which can easily provide exact gradient value at the point where gradient estimation is performed. Two kinds of test functions are introduced: a quadratic function

$$\phi = r^2 = x^2 + y^2 \quad (3.1)$$

and a linear function

$$\phi = x + 2y + 0.5. \quad (3.2)$$

Accordingly, exact gradient value in x, y and z directions can be obtained conveniently for the quadratic function

$$\begin{aligned} \frac{\partial \phi}{\partial x} &= 2x, \\ \frac{\partial \phi}{\partial y} &= 2y, \\ \frac{\partial \phi}{\partial z} &= 2z. \end{aligned} \quad (3.3)$$

and for the linear function

$$\begin{aligned} \frac{\partial \phi}{\partial x} &= 1, \\ \frac{\partial \phi}{\partial y} &= 2, \\ \frac{\partial \phi}{\partial z} &= 3. \end{aligned} \quad (3.4)$$

When the numerical test is conducted in three-dimensional case with more complex grid configuration, following test functions are considered

$$\phi = r^2 = x^2 + y^2 + z^2 \quad (3.5)$$

$$\phi = x + 2y + 3z + 0.5. \quad (3.6)$$

with exact gradient values calculated in the same manner as the two-dimensional situation. Herewith, aforementioned grid and test function types are denoted in a combined manner for simplicity, referring to the Table 3.1. For example, if the CWLSQ is examined on randomly diagonalized triangular grid with quadratic test function, this test case will be called R-Q.

Figure 3.1 Notation of grid and test function types

	Type	Notation
Grid	Quadrilateral grid	Q
	Uniformly diagonalized triangular grid	U
	Randomly diagonalized triangular grid	R
	Mixed grid	M
	Unstructured NACA0012 grid	N
Test Function	Quadratic function	Q
	Linear function	L

Meanwhile, gradient errors are evaluated at each grid cell

$$\text{Gradient error at the cell } i = e_i = \left| \frac{\nabla\phi_{i,exact} - \nabla\phi_{i,estimated}}{\nabla\phi_{i,exact}} \times 100 \right|. \quad (3.7)$$

3.2 Observation

3.2.1 Quadrilateral grid with test functions

As for both Q-Q and Q-L test cases, all gradient estimation methods present good gradient accuracy, having less than 1% of error as depicted in Fig. 3.2. In fact, good gradient accuracy from GGSA and GGNA was pointed out by existing studies [2,6,15] that GG type methods show its strength in viscous boundary layer grid. Surprisingly enough, however, one should note that LSQ types methods with inverse distance weighting function give even more accurate gradient compared to GG type methods.

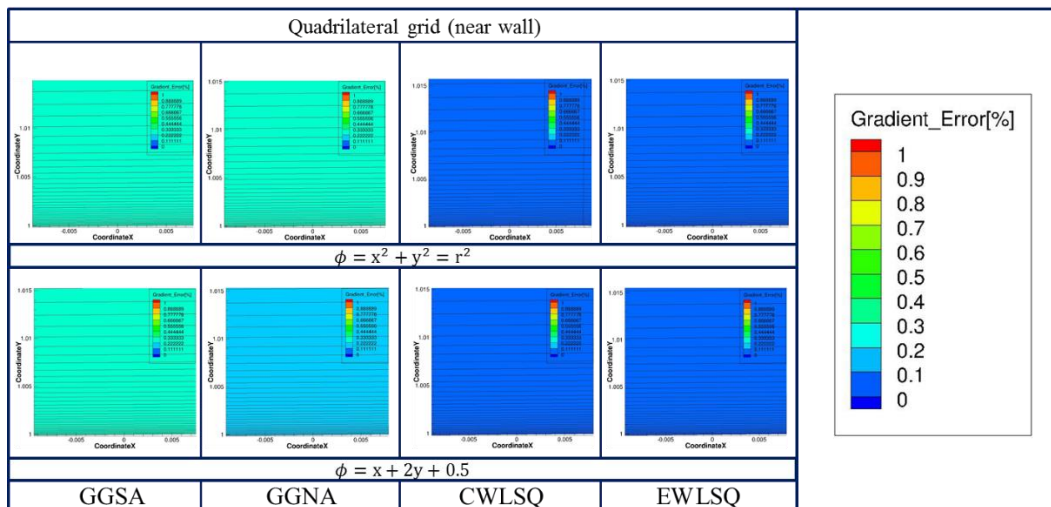


Figure 3.2 Comparison of results from quadrilateral grid

Moreover, as for Q-L test case, CWLSQ and EWLSQ are superior in terms of gradient accuracy, showing almost $O(10^{-10})$ magnitude of error, while GGSA and GGNA cannot reduce the gradient error under certain level due to their deficiency of linear-exactness. In

other words, two GG type methods are not able to reproduce the gradient value of the test function even if the function is linear. One-dimensional grid with non-uniform spacing is just enough to demonstrate this property [6], as shown in Fig. 3.3.

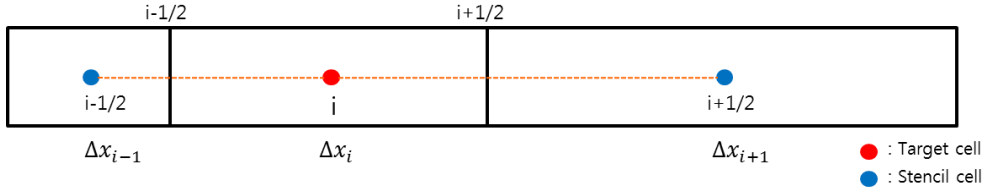


Figure 3.3 One-dimensional stencil configuration with non-uniform spacing

First, consider GGSA to estimate the gradient at the cell i

$$\nabla\phi_{i,GGSA} = \frac{1}{V} \sum_{k=1}^N \bar{\phi}_k \vec{n}_k A_k. \quad (3.8)$$

$$= \frac{\phi_{i+1/2} - \phi_{i-1/2}}{\Delta x_i}. \quad (3.9)$$

Cell-interface face values with simple averaging are

$$\phi_{i+1/2} = \frac{\phi_{i+1} + \phi_i}{2}, \quad (3.10)$$

$$\phi_{i-1/2} = \frac{\phi_i + \phi_{i-1}}{2}.$$

Inserting the Eq. (3.10) to Eq. (3.9), it leads to

$$\nabla\phi_{i,GGSA} = \frac{\phi_{i+1} - \phi_{i-1}}{2\Delta x_i} \quad (3.11)$$

where ϕ_{i+1} , ϕ_{i-1} are obtained from Taylor series expansion with respect to ϕ_i , i.e.,

$$\phi_{i+1} = \phi_i + \nabla\phi_i \left(\frac{\Delta x_{i+1} + \Delta x_i}{2} \right) + \frac{\nabla^2\phi_i}{2!} \left(\frac{\Delta x_{i+1} + \Delta x_i}{2} \right)^2 + O(h^3) \quad (3.12)$$

$$\phi_{i-1} = \phi_i - \nabla\phi_i \left(\frac{\Delta x_i + \Delta x_{i-1}}{2} \right) + \frac{\nabla^2\phi_i}{2!} \left(\frac{\Delta x_i + \Delta x_{i-1}}{2} \right)^2 + O(h^3)$$

Substituting the Eq. (3.12) to Eq. (3.11) and rearranging the equation, we obtain

$$\begin{aligned} \nabla\phi_{i,GGSA} &= \nabla\phi_i \left(\frac{1}{2} + \frac{\Delta x_{i+1} + \Delta x_{i-1}}{4\Delta x_i} \right) + \nabla^2\phi_i \left(\frac{\Delta x_{i+1} - \Delta x_{i-1}}{8} + \frac{\Delta x_{i+1}^2 - \Delta x_{i-1}^2}{16\Delta x_i} \right) + O(h^2) \\ &= \nabla\phi_i + \nabla\phi_i \left(-\frac{1}{2} + \frac{\Delta x_{i+1} + \Delta x_{i-1}}{4\Delta x_i} \right) + O(h) \end{aligned} \quad (3.13)$$

Obviously, the leading error term in Eq. (3.13) is zeroth order, implying that gradient by GGSA is inherently inconsistent method. Provided that $\Delta x_{i-1} = \Delta x_i = \Delta x_{i+1}$, which means a regular and uniform grid, GGSA can yield a second-order accurate gradient

$$\nabla\phi_{i,GGSA} = \nabla\phi_i + O(h^2). \quad (3.14)$$

However, this condition is far from the practical grid configuration encountered in actual CFD problem.

Likewise, applying the same procedure above to GGNA, it leads to

$$\begin{aligned} \nabla\phi_{i,GGNA} &= \frac{\nabla\phi_i}{2} \left[\frac{\Delta x_i(\Delta x_{i+1} + \Delta x_i)}{\Delta x_{i+1}^2 + \Delta x_i^2} + \frac{\Delta x_i(\Delta x_i + \Delta x_{i-1})}{\Delta x_i^2 + \Delta x_{i-1}^2} \right] \\ &\quad + \frac{\nabla^2\phi_i}{8} \left[\frac{\Delta x_i(\Delta x_{i+1} + \Delta x_i)^2}{\Delta x_{i+1}^2 + \Delta x_i^2} - \frac{\Delta x_i(\Delta x_i + \Delta x_{i-1})^2}{\Delta x_i^2 + \Delta x_{i-1}^2} \right] + O(h^2) \\ &= \nabla\phi_i + \frac{\nabla\phi_i}{2} \left[\frac{\Delta x_i(\Delta x_{i+1} + \Delta x_i)}{\Delta x_{i+1}^2 + \Delta x_i^2} + \frac{\Delta x_i(\Delta x_i + \Delta x_{i-1})}{\Delta x_i^2 + \Delta x_{i-1}^2} - 2 \right] + O(h). \end{aligned} \quad (3.15)$$

Even for this case, unless $\Delta x_{i-1} = \Delta x_i = \Delta x_{i+1}$ is satisfied, same conclusion as GGSA is attained. Therefore, these two GG type methods should not be preferred in actual flow

problem where irregular and mixed grids are dominant, especially when accurate gradient value itself is important, such as turbulence modeling.

3.2.2 Results by Green-Gauss type methods

As for all other grid and test function combination, such as U-Q, U-L, R-Q, etc., GG type methods exhibit large gradient error due to the fact demonstrated in earlier chapter. Even though GGNA show better accuracy than GGSA on mixed and unstructured NACA0012 grid, still the level of gradient accuracy is not satisfactory.

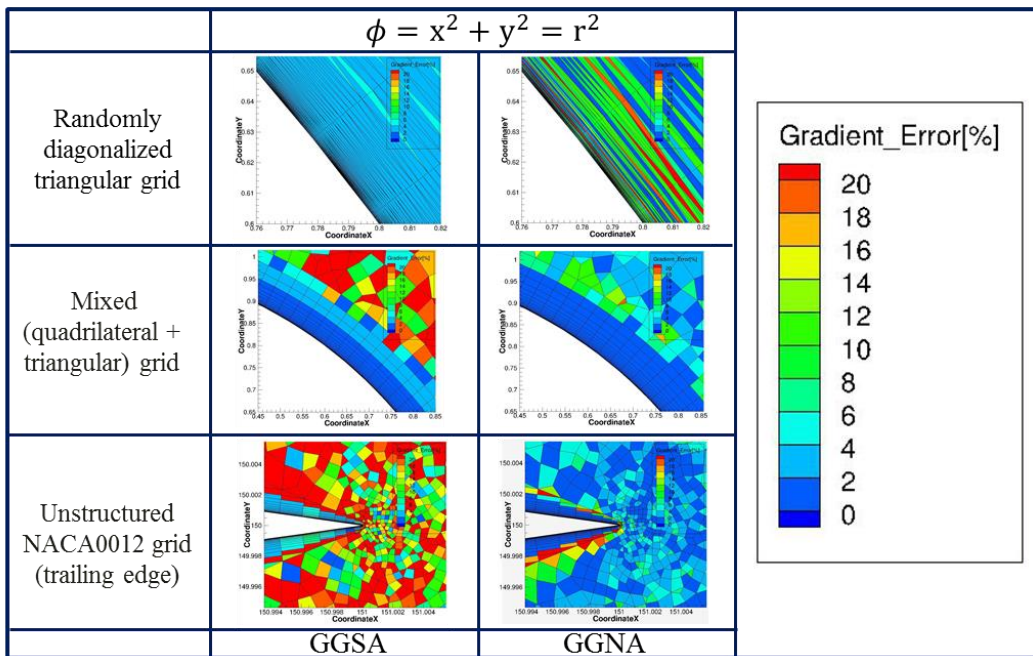


Figure 3.4 Contours of gradient error on triangular and mixed grid by GGSA and GGNA

3.2.3 Results by Least-Square type methods

Regarding the U-Q and R-Q test cases estimated by CWLSQ, cells with high gradient error exist, though accounting for less than 10% of entire cells. On the other hands, EWLSQ can successfully estimate the gradient, showing less than 1% of error for these cases. Comparison of gradient error by CWLSQ and EWLSQ for R-Q test case can be found in Fig. (3.5). Result of U-Q test case is line with that of R-Q and is omitted here. Except for the U-Q and R-Q case, both CWLSQ and EWLSQ show similar level of gradient accuracy.

EWLSQ, whose gradient accuracy is better than other methods investigated, usually require more than two to dozens of times more stencil than CWLSQ, and thus inevitably consumes more computational cost than the counterpart. However, as pointed out in M-Q and N-Q test cases, CWLSQ can yield comparable level of gradient accuracy in certain instances.

To sum up, at the viscous boundary layer, LSQ type methods can give even more accurate result than GG type methods, which turn out to be inherently inconsistent. Other grid, test function combination also showed that GG type methods are not suitable for general grid type, so one should refrain from applying them to actual flow simulation, especially where correct gradient value is crucial. Meanwhile, EWLSQ can provide accurate gradient for all test cases, and CWLSQ is comparable to EWLSQ except for U-Q and R-Q test cases. Therefore, by taking advantage of the merits of two LSQ approaches, which are relatively good gradient accuracy of EWLSQ and relatively low computational cost of CWLSQ with fair accuracy, and by switching between them depending on certain criterion, we can come up with an accurate and efficient gradient estimation method that

can be implemented on general unstructured grid.

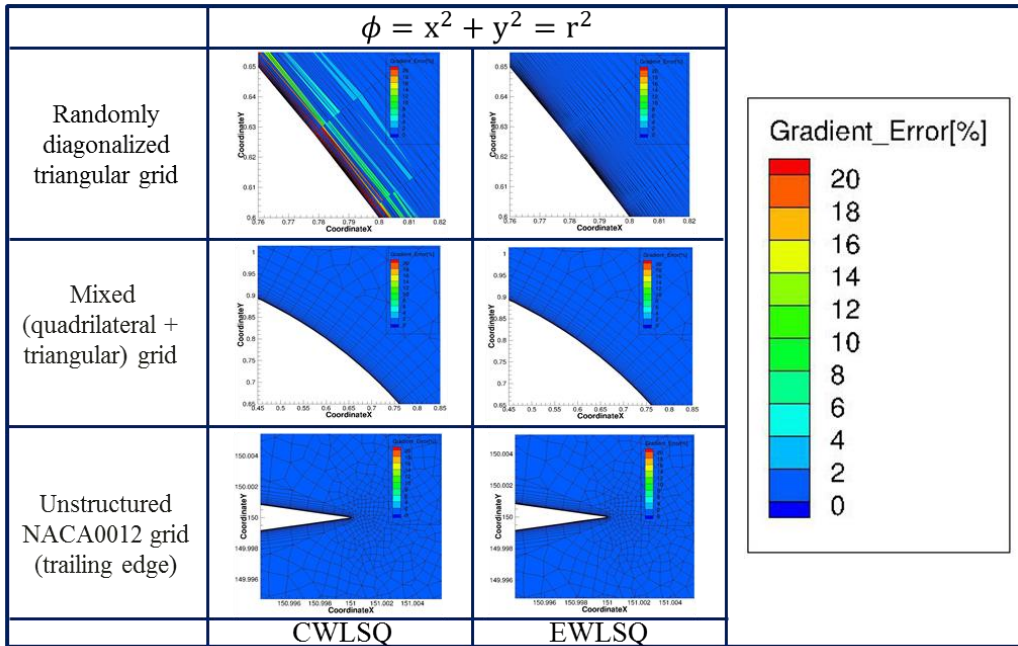


Figure 3.5 Contours of gradient error on triangular and mixed grid by GGSA and GGNA

Chapter 4

Least-Square Method Switching Function

4.1 Motivation

From the observation made in earlier chapter, we can think of an accurate and efficient gradient estimation method by switching between two LSQ methods. In other words, if the gradient error of a cell goes over the threshold, this cell adopts the EWLSQ for estimating the gradient, whose gradient accuracy was shown to be best among the candidates. Otherwise, the cell chooses CWLSQ as the gradient estimation method, who yields fair gradient accuracy and claims less computational cost compared to EWLSQ. However, to implement this idea on universal unstructured grid, we need to determine a consistent switching criterion which is solely dependent on grid information. In next sub-chapters, a consistent criterion for switching procedure will be discussed, resulting in the Switching Weighted Least-Square method (SWLSQ), followed by demonstration of SWLSQ around simple geometry.

4.2 Switching Criterion

4.2.1 Conventional Grid Quality Criterion

Conventionally, quality of the grid has been judged by parameters such as the aspect ratio, skewness and area (or volume) ratio. The aspect ratio of a grid cell is defined by the ratio of maximum to minimum length, and the skewness (or equiangle skewness) is defined by

$$\max \left[\frac{(Q_{max} - Q_e)}{(180 - Q_e)}, \frac{(Q_e - Q_{min})}{Q_e} \right] \quad (4.1)$$

with Q_{max} the largest, Q_{min} the smallest angle of a cell in degrees and Q_e angle for equilateral element in degrees. Meanwhile, the area ratio is calculated as follows

$$\max[\text{Size}(i)/\text{minSize}(j), \text{maxSize}(j)/\text{Size}(i)] \quad (4.2)$$

where $\text{Size}(i)$ denotes the area or volume of the cell, and $\text{minSize}(j)$ stands for minimum area or volume of the adjacent cell j . $\text{MaxSize}(j)$ denotes the maximum in the same range as $\text{minSize}(j)$.

Firstly, as a basic approach, these grid quality criteria are considered to find the correlation between the gradient error and them. Facts that these criteria are just function of geometric information of given grid and requires little effort are advantages of trying them as a switching criterion. Fig. 4.1 exhibits graphs of the gradient error versus conventional grid quality criteria estimated by CWLSQ on randomly diagonalized triangular grid. Clearly, however, none of the criteria shows direct proportionality

regarding the gradient error. For example, when it comes to the grid skewness, the gradient error stays low even if the skewness increases, before it reaches about 0.9. However, the error suddenly soars around 0.9.

Another radical disadvantage of taking conventional grid quality criteria as the switching threshold is that these criteria are basically confined to inspection of the target cell itself. For instance, think about a situation where a good quality cell encompassed by bad quality cells, and take the skewness of the cell as the switching criterion. Although the grid quality of the surrounding cells is bad, requiring extended stencil, since quality of the target cells is good, the target cell definitely adopts compact stencil, resulting in poor gradient accuracy. This is because gradient by Least-Square methods are affected stencil topology around the cell rather than the grid quality of the cell itself. Therefore, we need to set a criterion that can include the stencil information around the cell.

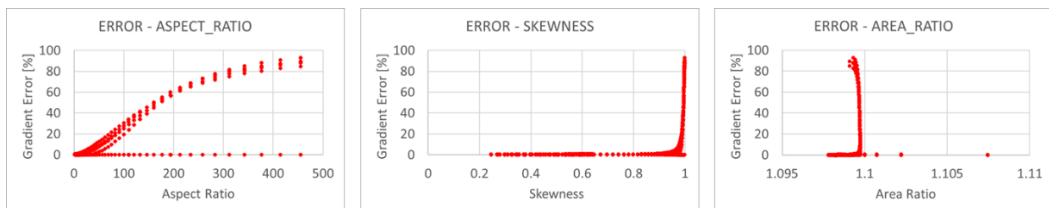


Figure 4.1 Gradient error with respect to conventional grid quality criteria

4.2.2 Condition Number of Least-Square Matrix

In linear algebra, condition number of the system measures how sensitive the output value is to the small change in the input. With respect to the Least-Square problem as in chapter 2

$$\begin{bmatrix} \sum_j^N w_j (\Delta x_j)^2 & \sum_j^N w_j \Delta x_j \Delta y_j & \sum_j^N w_j \Delta x_j \Delta z_j \\ \sum_j^N w_j \Delta x_j \Delta y_j & \sum_j^N w_j (\Delta y_j)^2 & \sum_j^N w_j \Delta y_j \Delta z_j \\ \sum_j^N w_j \Delta x_j \Delta z_j & \sum_j^N w_j \Delta y_j \Delta z_j & \sum_j^N w_j (\Delta z_j)^2 \end{bmatrix} \begin{bmatrix} \left(\frac{\partial \phi}{\partial x}\right)_i^* \\ \left(\frac{\partial \phi}{\partial y}\right)_i^* \\ \left(\frac{\partial \phi}{\partial z}\right)_i^* \end{bmatrix} = \begin{bmatrix} \sum_j^N w_j \Delta x_j \Delta \phi_{ij} \\ \sum_j^N w_j \Delta y_j \Delta \phi_{ij} \\ \sum_j^N w_j \Delta z_j \Delta \phi_{ij} \end{bmatrix} \quad (4.3)$$

, or shortly

$$\bar{A} \vec{x}^* = \vec{b}, \quad (4.4)$$

the condition number of Least-Square matrix \bar{A} can be interpreted as how sensitive the gradient \vec{x}^* is to the perturbation in the right-hand side of the Eq. (4.4) \vec{b} . In other words, the greater the perturbation, the larger the error becomes.

To observe correlation of the condition number and gradient error more intuitively, CWLSQ and EWLSQ are compared on U-Q and R-Q test cases, where major gradient accuracy gap was observed. Fig. 4.2 shows that the gradient error of CWLSQ continuously rises as the condition number increases on both grid types, while data of EWLSQ, low condition number and low gradient error, are clustered around 0 on the graph. The rationale for low and high condition number of each LSQ methods will be covered in next sub-chapter.

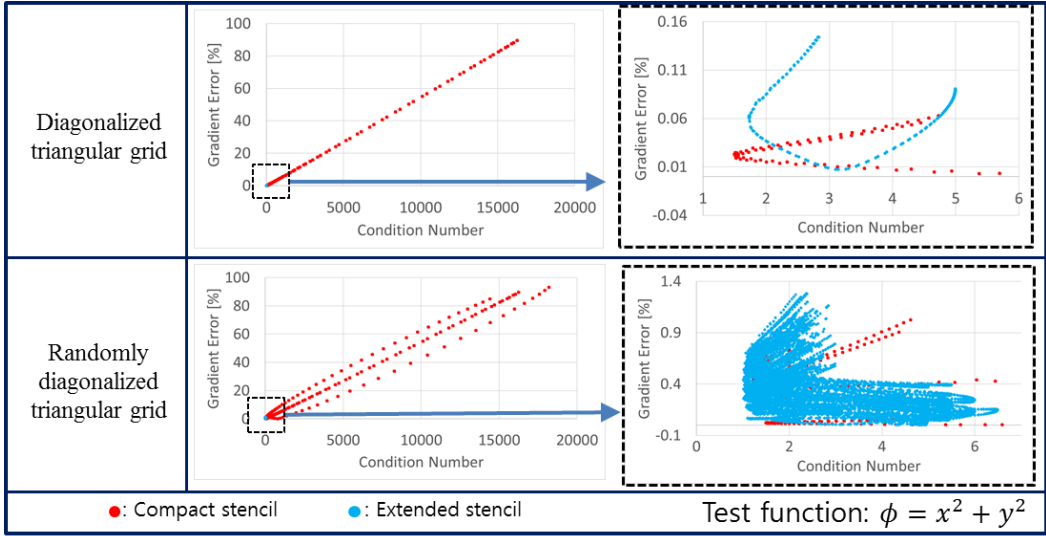


Figure 4.2 Comparison of two LSQ methods concerning the condition number and gradient error

$$\bar{A}\bar{x}^* = \sum_{j=1} w_j \Delta\bar{X}_j \Delta\phi_{ij} \quad (4.5)$$

where $\bar{X}_j = [\Delta x_j, \Delta y_j, \Delta z_j]$ is the vector from the target cell to the stencil. One should be reminded that the right-hand side of the Eq. (4.5) originally includes the second-order truncation error term $O(h^2)$

$$\bar{A}\bar{x}^* = \sum_{j=1} w_j \Delta\bar{X}_j \Delta\phi_{ij} + O(h^2). \quad (4.6)$$

, but this term is ignored during the Least-Square formulation. As a result, Least-Square method approximation has potential of impairing the gradient accuracy by nature, especially on ill-conditioned system. In other words, high condition number of the Least-

Square system indicates that the truncation error omitted will seriously damage the gradient accuracy.

In the same context, despite the high condition number of the Least-Square matrix, if the $O(h^2)$ is sufficiently low, then the gradient error will not be amplified, having accurate gradient. U-L and R-L test cases illustrated in Fig. 4.3 supports this argument. Even though the condition number by CWLSQ can be extremely high in both grid types, very low truncation error, bounded below $4.5E^{-10}$, hardly affects the gradient value, producing as low gradient error as EWLSQ.

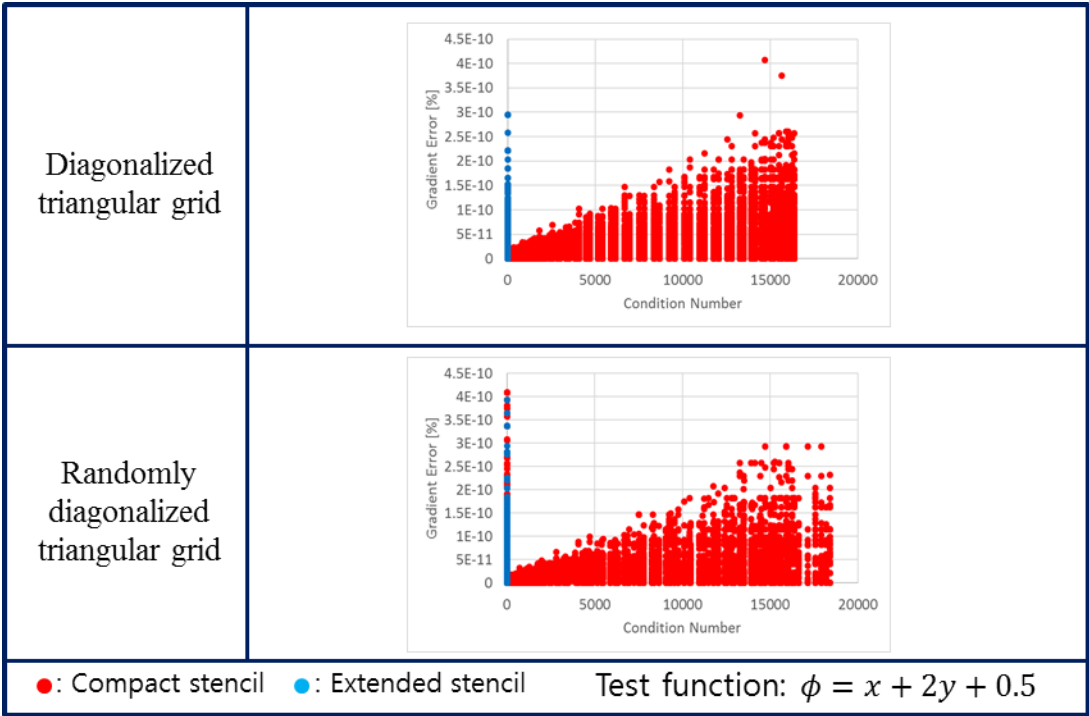


Figure 4.3 Comparison of CWLSQ and EWLSQ result from U-Q and R-Q test cases

Therefore, when Least-Square method with compact stencil shows unacceptable gradient accuracy, we should expand the stencil scope by adopting EWLSQ, and the condition number can be used as a criterion.

Another merit of usage of condition number is that the \bar{A} is only comprised of distance information from the target cell to neighboring cells which are purely geometric property, just as conventional grid quality parameters. Accordingly, one can pre-compute the condition number of the grid once and decide the range of the Least-Square method before the actual computation.

4.2.3 Condition Number Calculation Method

4.2.3.1 Quadratic Formula

As stated in previous sub-chapter, basic concept of the condition number is how much the output value changes with respect to the perturbation in the input. More precisely, following the notation in Eq. (4.4), the condition number $k(\bar{A})$ can be defined as maximum ratio of the relative error in \vec{x}^* to the relative error in \vec{b}

$$k(\bar{A}) = \frac{\|\bar{A}^{-1}e\|/\|\bar{A}^{-1}\vec{b}\|}{\|e\|/\|\vec{b}\|} \quad (4.7)$$

with e and $\|\bar{A}^{-1}e\|$ standing for relative error in \vec{b} and error in the solution $\|\bar{A}^{-1}\vec{b}\|$ respectively. The Eq. (4.7) is also same as

$$k(\bar{A}) = \left(\frac{\|\bar{A}^{-1}e\|}{\|e\|} \right) \left(\frac{\|\vec{b}\|}{\|\bar{A}^{-1}\vec{b}\|} \right) \quad (4.8)$$

for nonzero \vec{b} and e . The maximum value of Eq. (4.8) is obtained by product of two terms as follows

$$k(\bar{A}) = \max_{e \neq 0} \left(\frac{\|\bar{A}^{-1}e\|}{\|e\|} \right) \cdot \max_{b \neq 0} \left(\frac{\|\vec{b}\|}{\|\bar{A}^{-1}\vec{b}\|} \right) \quad (4.9)$$

$$= \max_{e \neq 0} \left(\frac{\|\bar{A}^{-1}e\|}{\|e\|} \right) \cdot \max_{b \neq 0} \left(\frac{\|\bar{A}\vec{x}^*\|}{\|\vec{x}^*\|} \right) \quad (4.10)$$

$$= \|\bar{A}^{-1}\| \cdot \|\bar{A}\| \quad (4.11)$$

where $\|\cdot\|$ denotes the L-2 norm of a vector or matrix.

Least-Square matrix \bar{A} is a normal matrix, satisfying the condition below

$$\bar{A} \bar{A}^T = \bar{A}^T \bar{A}, \quad (4.11)$$

with superscript T denoting the transpose of a real matrix, or conjugate transpose for a complex matrix. Therefore, the condition number can be also acquired from the maximum to minimum eigenvalue λ ratio as

$$k(\bar{A}) = \frac{|\lambda_{\max}(\bar{A})|}{|\lambda_{\min}(\bar{A})|} \quad (4.12)$$

As for a two-dimensional case, two eigenvalues of the \bar{A} can be readily obtained from the quadratic formula applied to the characteristic polynomial, i.e, $\det(\bar{A} - \lambda I)$, because the eigenvalues are roots of the characteristic polynomial.

4.2.3.2 Power Method

As for a three-dimensional case, where \bar{A} is a 3×3 matrix, calculating the condition number from the roots of the characteristic polynomial is limited since, general solution for the cubic equation is more complex and contains imaginary values. Fortunately, however, we can get the maximum and minimum eigenvalues of the system in an iterative manner by applying so called Power Method.

Given a diagonalizable \bar{A} , and \vec{z} , which approximates the dominant eigenvector or simply a random vector, Power Method is performed as

$$\vec{z}^1 = \bar{A} \vec{z}^0 \quad (4.13)$$

$$\vec{z}^1 = \frac{\vec{z}^1}{|\vec{z}^1|}$$

$$\vec{z}^2 = \bar{A}\vec{z}^1$$

...

$$\vec{z}^{n+1} = \bar{A}\vec{z}^n$$

where the superscript over the \vec{z} denotes the iteration step. One should be careful that equal sign in Eq. (4.13) stands for the insertion of the right-hand side value to the left-hand side value, commonly used concept in computer science. After enough iterations, \vec{z}^n becomes the greatest eigenvalue of \bar{A} . Applying the same procedures as in Eq. (4.13) to \bar{A}^{-1} instead of \bar{A} , one gets the reciprocal of the minimum eigenvalue of \bar{A} . Another point to keep in mind is that the calculated maximum and minimum eigenvalues are the greatest and the smallest eigenvalues in absolute value.

4.3 Switching Least-Square Method

4.3.1 Behavior of Condition Number of CWLSQ and EWLSQ

From the earlier sub-chapters, we can understand why the condition number of the Least-Square matrix is an appropriate candidate for the switching criterion and how to calculate the condition number in two and three-dimensional situations. Remaining questions is then, for a given grid, why EWLSQ presents low condition number, thus leading to low gradient error, and CWLSQ causes ill-conditioned system. This phenomenon can be explained by expressing stencil configuration between the target cell and neighboring cells with trigonometric functions.

Consider a two-dimensional case where \bar{A} is a 2×2 matrix

$$\bar{A} = \begin{bmatrix} \sum_{j=1} w_j \Delta x_j^2 & \sum_{j=1} w_j \Delta x_j \Delta y_j \\ \sum_{j=1} w_j \Delta x_j \Delta y_j & \sum_{j=1} w_j \Delta y_j^2 \end{bmatrix} = \begin{bmatrix} a & b \\ c & d \end{bmatrix}. \quad (4.14)$$

Then the characteristic polynomial can be written as

$$(a - \lambda)(d - \lambda) - bc = 0 \quad (4.15)$$

, and from the quadratic formula, $k(\bar{A})$ is obtained as follows

$$k(\bar{A}) = \frac{|\lambda_{max}|}{|\lambda_{min}|} = \frac{(a + d) + \sqrt{(a - d)^2 + 4bc}}{(a + d) - \sqrt{(a - d)^2 + 4bc}} \quad (4.16)$$

Introducing trigonometric functions and identities, alternative expression for components of \bar{A} can be obtained as described in Fig. 4.4

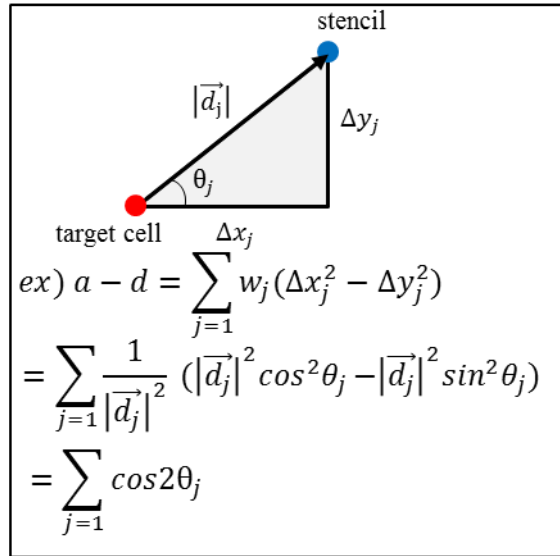


Figure 4.4 Alternative expression of components using trigonometric functions and identities

Applying the same process to terms $a + d$ and $4bc$ in Eq. (4.16)

$$a + d = \sum_{j=1} w_j (\Delta x_j^2 + \Delta y_j^2) \quad (4.17)$$

$$= N,$$

$$4bc = 4 \sum_{j=1} w_j \Delta x_j \Delta y_j \sum_{j=1} w_j \Delta x_j \Delta y_j$$

$$= 4 \sum_{j=1} \cos \theta_j \sin \theta_j \sum_{j=1} \cos \theta_j \sin \theta_j \quad (4.18)$$

$$= 4 \sum_{j=1} \frac{1}{2} \sin 2\theta_j \sum_{j=1} \frac{1}{2} \sin 2\theta_j$$

$$= \left(\sum_{j=1} \sin 2\theta_j \right)^2.$$

Collecting all alternative expressions, the condition number is derived as

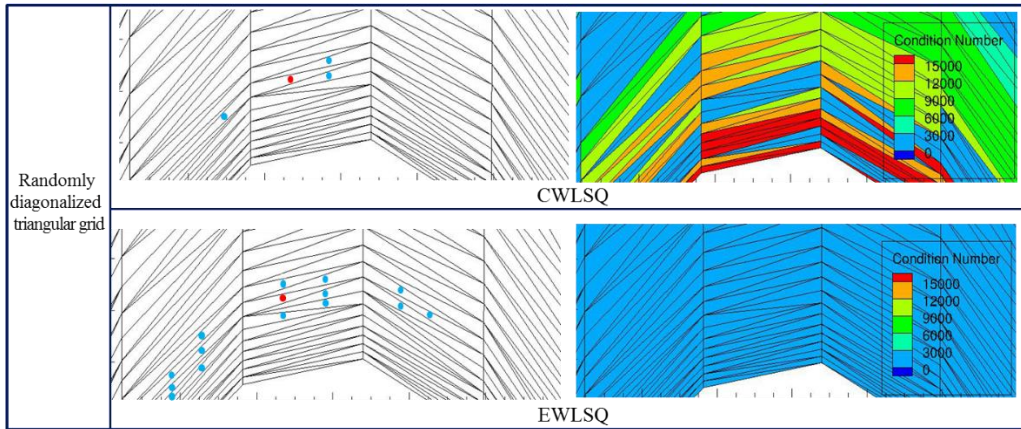
$$k(\bar{A}) = \frac{(a+d) + \sqrt{(a-d)^2 + 4bc}}{(a+d) - \sqrt{(a-d)^2 + 4bc}} = \frac{N + \sqrt{N+p}}{N - \sqrt{N+p}} \quad (4.19)$$

where N is the number of stencils, and p is function of angles of stencil vectors. Stencil vector is a vector originating from the centroid of the target cell to that of neighboring cell.

For example, p for four stencil vectors are expressed as

$$p = 2[\cos 2(\theta_1 - \theta_2) + \cos 2(\theta_1 - \theta_3) + \cos 2(\theta_1 - \theta_4) + \cos 2(\theta_2 - \theta_3) + \cos 2(\theta_2 - \theta_4) + \cos 2(\theta_3 - \theta_4)] \quad (4.20)$$

According to the new definition of the condition number, since EWLSQ takes about two to dozens of times more stencils encompassing the target cell, having greater N , $k(\bar{A})$ easily is mitigated, keeping low condition number. In contrast, CWLSQ is prone to cause high $k(\bar{A})$, leading to greater gradient error. This can be confirmed by an example of condition number calculation in Fig. 4.5. For the R-Q test case, EWLSQ takes about four times more stencils than CWLSQ. Although stencil configuration suggests that EWLSQ has greater p , larger N of EWLSQ successfully prevents $k(\bar{A})$ from being amplified.



$$k(A) = \frac{N + \sqrt{N + p}}{N - \sqrt{N + p}}$$

	N	p	$k(A)$	Error [%]
CWLSQ	3	2.9995	14434	68
EWLSQ	14	9.9952	6	0.14

Figure 4.5 Condition number calculation example of CWLSQ and EWLSQ

4.3.2 Switching Procedure

From the observation made in chapter 4.3.1, we can expect that EWLSQ consistently outperforms the CWLSQ by having overall lower condition number and gradient error regardless of types of the grid. Therefore, the maximum or average condition number of EWLSQ can be a good candidate for switching criterion value. However, choosing the maximum condition number of EWLSQ may have little merit in grids around simple geometry, but this criterion is vulnerable to a condition number overshoot witnessed around a practical and complex geometry, which will be discussed in later chapter. For simple demonstrations, however, both max and average condition number of EWLSQ are examined as the switching criterion. On the other hand, setting fixed value as switching

criterion cannot properly handle the condition number gap between different dimensions or geometry complexity. Thus, average condition number of EWLSQ is utilized as switching criterion, defining a Switching Weighted Least-Square method (SWLSQ).

Fig. 4.6 describes the overall process of SWLSQ. Firstly, compute the condition number of CWLSQ ($C k(A)$) and EWLSQ ($E k(A)$) for a given grid. Next, calculate the average condition of number of EWLSQ ($Avg E k(A)$) to set the criterion. Basically, CWLSQ is adopted as an initial gradient estimation method. With respect to a particular grid cell, if the $C k(A)$ is greater than switching criterion, then, this cell will be switched to EWLSQ. Otherwise, the cell remains using the compact stencil.

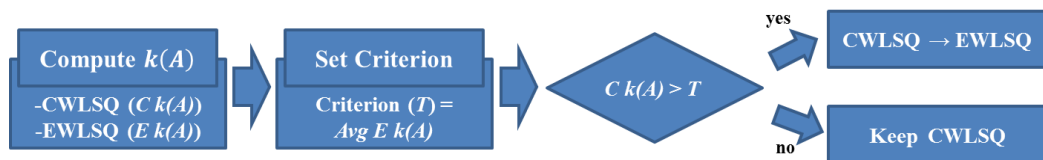


Figure 4.6 Overall procedure of SWLSQ

4.4 Simple Demonstration

4.4.1 Two-Dimensional Randomly Diagonalized Triangular Grid

Consistent switching criterion defined in earlier chapter is applied to R-Q test case to demonstrate its usefulness. The results from three LSQ methods are summarized in Fig. 4.7 where $Max E k(A)$, maximum condition number of EWLSQ, is applied as switching criterion. The maximum condition number and average condition number of EWLSQ are 7 and 3.6 respectively. When average condition number is applied as the switching criterion, about 5% of more cells are converted compared to the case where the maximum condition number is used. Seeing from the Fig. 4.7, where $Max E k(A)$ sufficiently works well, it may give an impression that using average $Avg E k(A)$ unnecessarily change more cells required. However, drawback of using $Max E k(A)$ as the switching criterion will be revealed in next chapter.

When CWLSQ is applied on R-Q test case, maximum gradient error obviously goes beyond the acceptable accuracy level, but this can be successfully controlled by using SWLSQ, showing about 1.28% of maximum error.

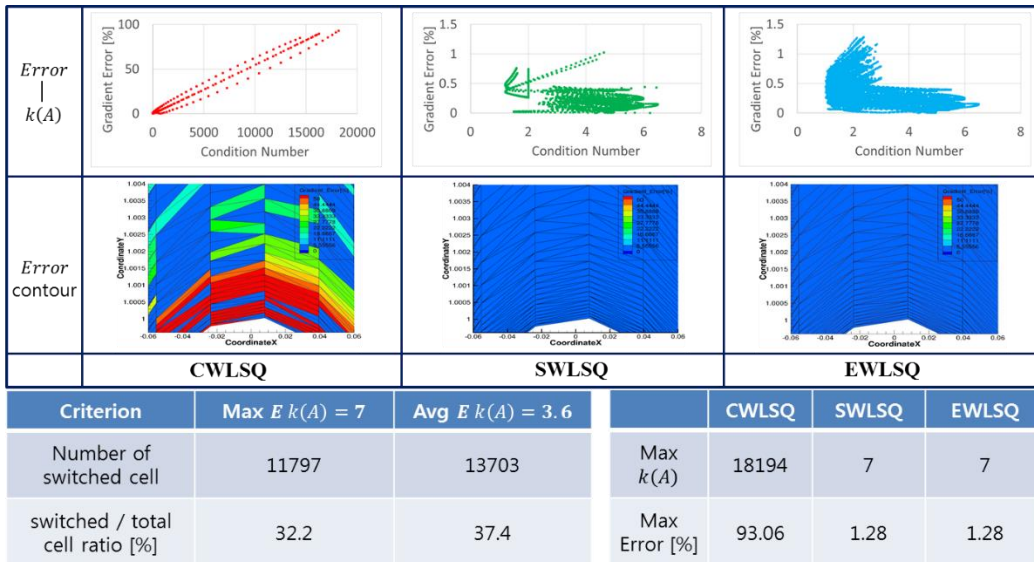


Figure 4.7 Comparison of three LSQ methods on R-Q test case

4.4.2 Three-Dimensional Random tetrahedral Grid

For three-dimensional simple demonstration case, random tetrahedral grid around a sphere together with quadratic test function are employed. As the two-dimensional test case, $Max E k(A)$ is applied as the switching criterion for this simple case. Although $Avg E k(A)$ condition number changes about 5% more cells from CWLSQ to EWLSQ, just like the R-Q test case, but this figure is not important compared to the stability issue of $Max E k(A)$. When CWLSQ alone is applied, the gradient accuracy is totally collapsed, showing over 400% of error. However, SWLSQ can cure this phenomenon giving about 4% of maximum error, which is similar to that of EWLSQ.

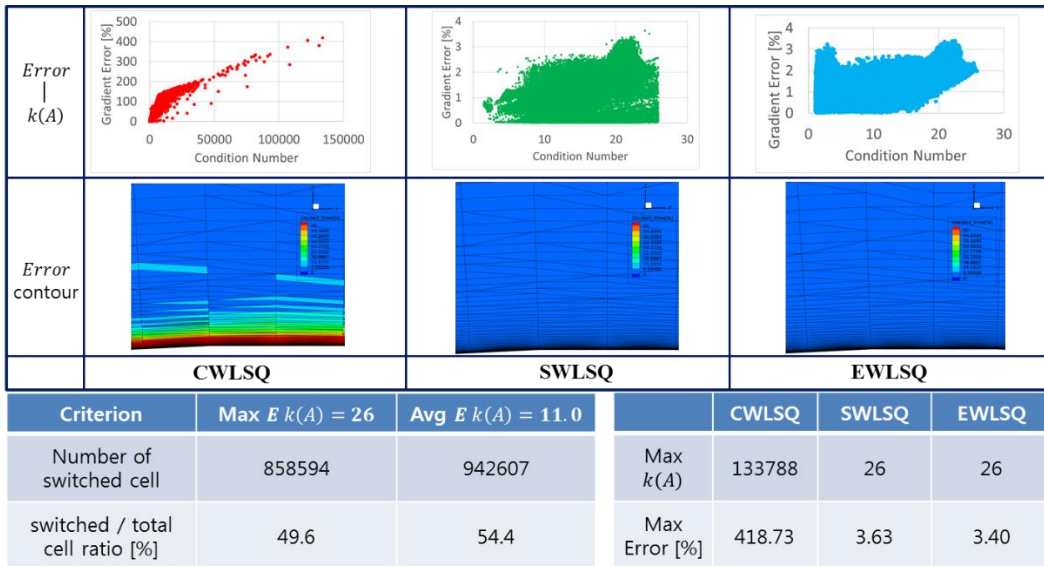


Figure 4.8 Comparison of three LSQ methods on three-dimensional test case

Chapter 5

Application

5.1 Two-Dimensional NACA0012 Airfoil

In this chapter, the switching criterion established is applied to more practical and/or complex geometry. For the first test case, SWLSQ is applied to two-dimensional NACA0012 Airfoil, which is usually considered as a typical demonstration case. A summary of numerical schemes and information of the flow simulation are listed in Table 5.1. Since the overall grid quality around NACA0012 is good, about less than 1% of cells were switched from compact stencil to extended stencil, meaning that most cell virtually employ CWLSQ for gradient estimation.

Table 5.1 Summary of information of the flow simulation over NACA0012

Simulation Information	Value
Mach Number	0.5
Angle of Attack	1.25
Reynolds Number	1.1×10^7
Flow Type	Turbulent Flow
Turbulence model	Menter's k-w SST
Convective flux	RoeM [16]
Time Integration Method	Implicit Euler
Linear Algebra Method	LU-SGS

As can be seen from the pressure coefficient over the NACA0012 in Fig. 5.1, all three LSQ methods produces almost same result, and only one pressure contour around the airfoil is posted in Fig. 5.1 for brevity. Nevertheless, one should note that SWLSQ costs about 18%

less computation time compared to EWLSQ, showing SWLSQ is working well in simple demonstration problem.

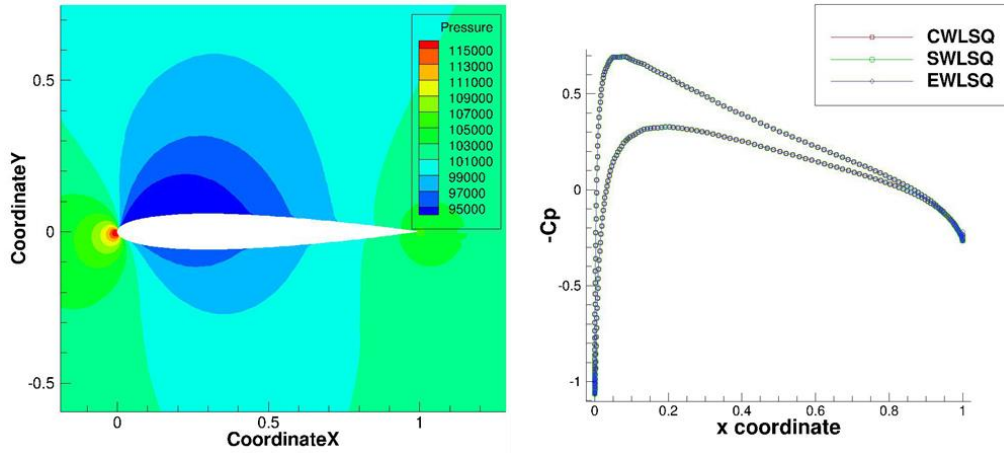


Figure 5.1 Comparison of three LSQ methods on two-dimensional NACA0012

5.2 Three-Dimensional Wing-Body Configuration

5.2.1 Test Function

Three-Dimensional wing-body configuration, or common research model (CRM), is used to verify the usefulness of the SWLSQ. As like the airfoil test case, SWLSQ is compared with other two LSQ methods, CWLSQ and EWLSQ. However, different from the earlier application, firstly, three LSQ methods are compared using quadratic test function to check the gradient accuracy.

We mention here that when $Max Ek(A)$ is applied as the switching criterion, it fails to compute flow quantities during the computation. This is because even if EWLSQ is used for gradient estimation, there are cells that presents abnormally high condition number, usually found near the boundary cells due to unusual stencil distribution. These cells make switching criterion too high that only few cells are switched to EWLSQ, about 2.5% in this case. As a result, cells with high condition number and gradient error still linger, spoiling the entire flow simulation. Therefore, $Avg Ek(A)$ is implemented as the switching criterion from now on for stability issue.

As for CRM, when CWLSQ is used, cells with poor gradient accuracy and high condition number are found near the trailing edge of the wing as illustrated in Fig 5.2. Maximum gradient error soars over 260% which is unacceptable amount of figure in real application. When SWLSQ with $Avg Ek(A)$ as the switching criterion is applied, about 22% of cells are switched from CWLSQ to EWLSQ, reducing the maximum gradient error from about 270% to 9.6%. This can be confirmed in the error and condition number contour

near the trailing edge in Fig 5.2. High gradient error region observed in CWLSQ are effectively cured when SWLSQ is utilized.

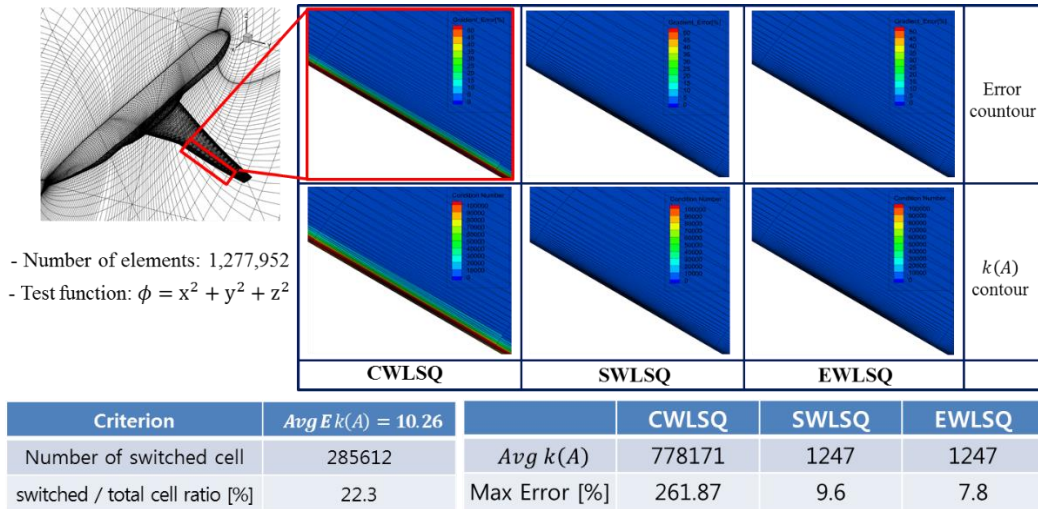


Figure 5.2 Comparison of three LSQ methods on the CRM

5.2.2 Flow Simulation

Three LSQ methods are employed to conduct the flow simulation over the CRM. Information about the numerical schemes and other inputs are listed in Table 5.2. As expected from the high gradient error of CWLSQ, observed in earlier chapter, CWLSQ fails to compute this test case. In contrast, SWLSQ successfully computes this case, saving about 10% computation time compared to EWLSQ. Even though lift and drag coefficients calculated from SWLSQ show little deviation from that of EWLSQ, the error is 0.12% for C_L and 0.35% for C_D . Pressure contour of both SWLSQ and EWLSQ over the CRM are almost same that only one of them is posted as in Fig 5.3.

Table 5.2 Summary of information of the flow simulation over the CRM

Simulation Information	Value
Mach Number	0.85
Angle of Attack	2.3
Reynolds Number	5.1×10^6
Flow Type	Turbulent Flow
Turbulence model	Menter's k-w SST
Convective flux	AUSMPW+ [17]
Time Integration Method	Implicit Euler
Linear Algebra Method	GMRES

Table 5.3 Aerodynamic coefficients and computation time of two LSQ methods

LSQ Method	SWLSQ	EWLSQ	Error [%]
C_L	0.5042	0.5036	0.12
C_D	0.0288	0.0287	0.35
Computation Time [sec]	37810	41613	-

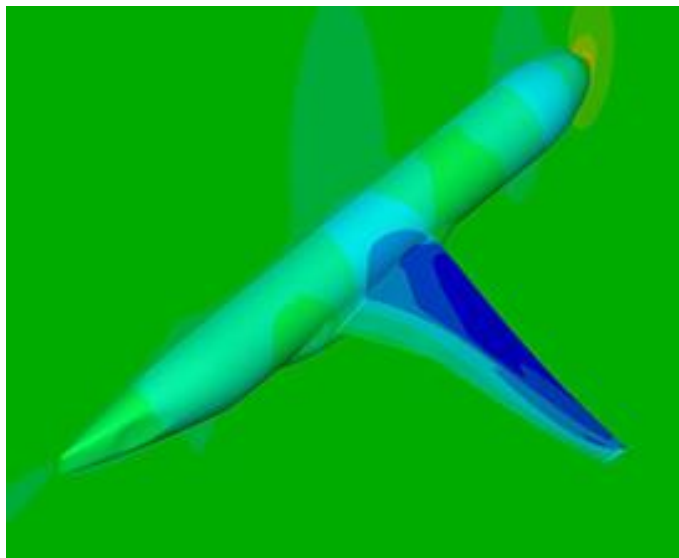


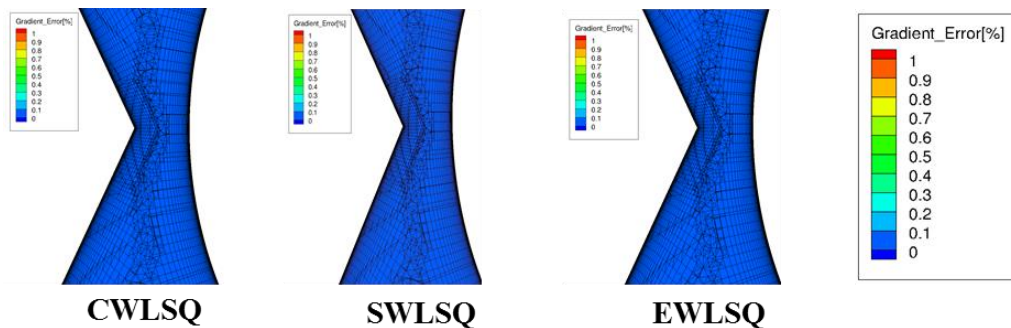
Figure 5.3 Pressure contour of the CRM

5.3 Modern Fighter

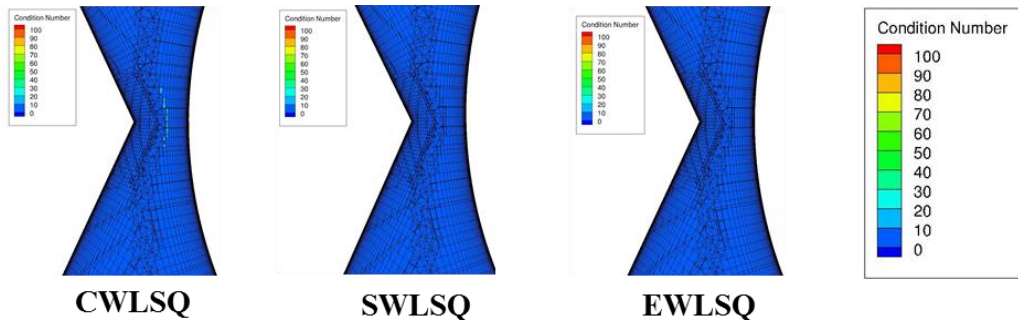
5.3.1 Test Function

To present the gradient accuracy and computational efficiency of the SWLSQ on more pragmatic and complex geometry, a modern fighter configuration is adopted. SWLSQ is compared with other two Least-Square methods, CWLSQ and EWLSQ.

Test function examined on previous chapters, $\phi = x^2 + y^2 + z^2$, is utilized again for consistent application. At each cell, the estimated gradient by SWLSQ is compared with exact gradient value, which can be obtained from known test function. Fig 5.4 illustrates the first-gradient error and condition number of each Least-Square method at the region where poor gradient accuracy triggered the numerical oscillation, mentioned in introduction of this work. Unfortunately, however, no sensible difference between three Least-Square methods exist in Fig 5.4(a) regarding the first-gradient error, showing less than 1% error in all cases. Only minor condition number overestimation is observed in case of CWLSQ in Fig 5.4(b).



(a) First-gradient error



(b) Condition number

Figure 5.4 Comparison of three Least-Square methods

However, in contrast with the first-gradient, contour of the second-gradient of Least-Square methods in Fig 5.5 present distinct difference, characterized by cells with large error by CWLSQ. Although it is obvious that these cells with bad gradient accuracy are attributed to numerical oscillation, switching criterion proposed in previous chapter cannot help CWLSQ to be switched to EWLSQ effectively, supported by the fact that red cells are still left in the contour of SWLSQ. This suggests that further research is required to figure out the connection between the second-gradient and the condition number of the Least-Square matrix for appropriate switching mechanism.

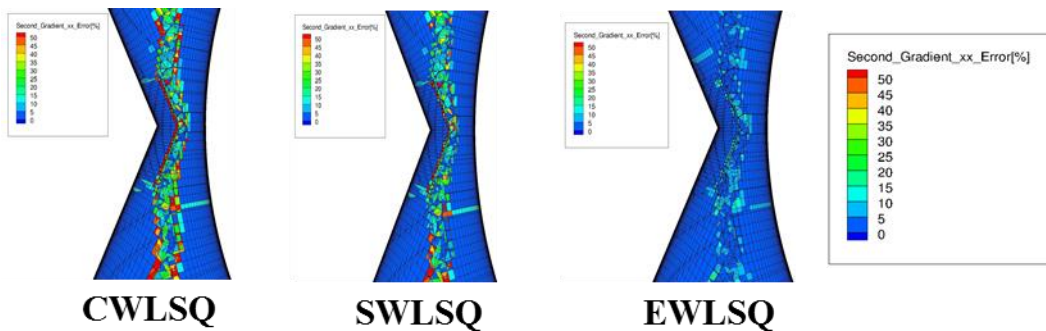


Figure 5.5 Comparison of second-gradient error of three Least-Square methods

5.3.2 Flow Simulation

In order to analyze the effect of second-gradient accuracy on each Least-Square method, actual flow simulation over the fighter is conducted. The numerical schemes and basic information of the flow simulation are summarized in Table 5.4.

Table 5.4 Summary of information of the flow simulation over the fighter

Simulation Information	Value
Mach Number	0.95
Angle of Attack	17.0
Reynolds Number	3.5×10^6
Flow Type	Turbulent Flow
Turbulence model	Menter's k-w SST
Convective flux	RoeM
Time Integration Method	Implicit Euler
Linear Algebra Method	GMRES

As expected from the result of previous sub-chapter, CWLSQ, which exhibits large second-gradient error, fails to compute this case. Convergence history of calculated lift coefficient and drag coefficient of SLWSQ and EWLSQ are plotted in Fig 5.6, showing that SWLSQ gives almost same result as EWLSQ. Meanwhile, the number and ratio of switched cell among the total number of cells are listed in Table 5.5. In addition, the error of lift and drag coefficients of SWLSQ and computation time are shown in Table 5.6. Specific aerodynamic coefficient values, as well as the full configuration of the modern fighter, are omitted here for confidentiality policy. One should note that SWLSQ successfully computes this case and saves almost 32% of computation time compared to EWLSQ, compromising only less than 1% of accuracy of aerodynamic coefficients.

Table 5.5 The number and ratio of switched cells

Criterion Value	4.62126
Number of Switched / Total Cell	4619304 / 68687966
Ratio of Switched / Total Cell [%]	6.7

Table 5.6 Lift and drag coefficient error of SWLSQ and comparison of computation time

LSQ Method	SWLSQ	EWLSQ
C_L Error [%]	0.64	-
C_D Error [%]	0.60	-
Computation Time [hr]	68.18	99.59

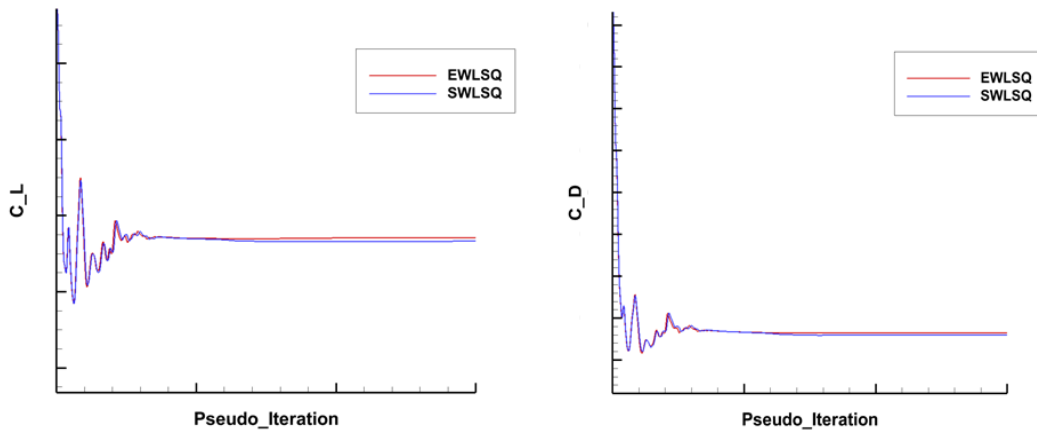


Figure 5.6 Comparison of second-gradient error of the two Least-Square methods

Chapter 6

Conclusion

A switching Least-Square method exploiting the merits of two LSQ methods is proposed for accurate and efficient gradient estimation on general unstructured grid.

To begin with, two preceding gradient estimation categories are investigated, gradient by Green-Gauss theorem and gradient by Least-Square methods. It was found that Green-Gauss methods using simple averaging and node averaging for cell-interface value are inherently inconsistent. Meanwhile, Least-Square methods using proper inverse distance weighting function yield even more accurate gradient at viscous boundary layer grid than GG type methods. Therefore, GG type methods are not applied in further research. As for comparison of CWLSQ and EWLSQ, considering the fair gradient accuracy of CWLSQ and computational cost of EWLSQ, switching between two LSQ methods can lead to accurate and efficient gradient estimation method.

For consistent switching criterion that can be implemented on general unstructured grid, condition number of the Least-Square matrix is considered. This is because the condition number shows strong correlation with the gradient error, and it can be easily computed from the given grid in advance. By using the trigonometric functions, it is shown that LSQ method with extended stencil tends to have lower condition number, thus leading to lower gradient error because of greater number of stencils. Even though maximum condition

number of the EWLSQ seems to be a good candidate for switching criterion value, it exhibits a stability problem, caused by condition number overshoot at a region near the boundary of the grid. Therefore, eventually, average condition number of the EWLSQ is selected as the switching criterion.

Lastly, SWLSQ is applied to simple and complex grid to verify its excellence. In terms of gradient accuracy, SWLSQ produces similar level of accuracy compared to EWLSQ, saving about 10 to 30% computation time depending on the flow problem.

During the application of SWLSQ on complex grid around the modern fighter, it was found that the accuracy of the first-gradient is not a sufficient condition for the accurate estimation of the second-gradient. Therefore, future research is needed to understand the characteristics of second-gradient and to find proper methodologies that can estimate second-gradient.

References

- [1] Aftosmis, M., Gaitonde, D., Tavares, T. S., “Behavior of Linear Reconstruction Techniques on Unstructured Meshes,” *AIAA Journal*, Vol 33, No. 11, Nov 1995, pp. 2038-2049
- [2] Mavriplis, D. J., “Revisiting the Least-Square Procedure for Gradient Reconstruction on Unstructured Meshes,” AIAA Paper 2003-3986, June 2003
- [3] Diskin, B., Thomas, J. L., “Comparison of Node-Centered and Cell-Centered Unstructured Finite Volume Discretization: Inviscid Fluxes,” *AIAA Journal*, Vol. 49, No. 4, 2011, pp. 836-854
- [4] Correa, C. D., Hero, R., Ma, K., “A Comparison of Gradient Estimation Methods for Volume Rendering on Unstructured Meshes,” *IEEE Trans Vis Comput Graph*, Vol. 17, No. 3, March 2011, pp. 305-319
- [5] Shima, E., Kitamura, K., Fujimoto, K., “New Gradient Calculation Method for MUSCL Type CFD Schemes in Arbitrary Polyhedra,” AIAA 2010-1081, Jan 2010
- [6] Sozer, E., Brehm, C., Kiris, C., “Gradient Calculation Methods on Arbitrary Polyhedral Unstructured Meshes for Cell-Centered CFD Solvers,” AIAA 2014-1440, Jan 2014
- [7] Schwöppe, A., Diskin, B., “Accuracy of the Cell-Centered Grid Metric in the DLR TAU-Code,” *New Results in Numerical and Experimental Fluid Mechanics VIII*, Vol. 121, 2013, pp. 429-437
- [8] Petrovskaya, N., “The Accuracy of Least-Square Approximation on Highly Stretched Meshes,” *International Journal of Computational Methods*, Vol. 5, No. 3, 2008, pp.

- [9] White, J. A., Baurle, R. A., Passe, B. J., Spiegel, S. C., “Geometrically Flexible and Efficient Flow Analysis of High Speed Vehicles Via Domain Decomposition, Part 1, Unstructured-grid Solver for High Speed Flows,”
- [10] Syrakos, A., Varchanis S., Dimakopoulous, Y., Goulas, A., Tsamopoulos, J., “A Critical Analysis of Some Popular Methods for the Discretization of the Gradient Operator in Finite Volume Methods,” *Phys. Fluids* 29(2017) 127103
- [11] Anderson, W. K., Bonhaus, D. L., “An Implicit Upwind Algorithm for Computing Turbulent Flows on Unstructured Grids,” *Computers & Fluids*, Vol. 23, No. 1, 1994, pp. 1-21
- [12] Haselbacher, A., Blazek, J., “On the Accurate and Efficient Discretization of the Navier-Stokes Equations on Mixed Grids,” *AIAA Journal*, Vol. 38, No. 11, 2000, pp. 2094-2102
- [13] Blazek, J., “Unstructured Finite-Volume Schemes,” *Computational Fluid Dynamics: Principles and Applications*, 3rd ed., Butterworth-Heinmann, Kidlington, 2015, pp.121-162
- [14] Diskin, B., Thomas, J. L., “Accuracy of Gradient Reconstruction on Grids with High Aspect Ratio,” National Inst. of Aerospace Rept. NIA 2008-12, Hampton, VA, Dec 2008.
- [15] Shima, E., Kitamura, K., Haga, T., “Green-Gauss/Weighted Least-Squares Hybrid Gradient Reconstruction for Arbitrary Polyhedra Unstructured Grids,” *AIAA Journal*, Vol. 51, No. 11, 2013, pp. 2740-2747
- [16] Kim, S., Kim, C., Rho, O. H., Hong, S. K., “Cures for the Shock Instability:

- Development of a Shock-Stable Roe Scheme,” *Journal of Computational Physics*, Vol. 185, No. 2, 2003, pp. 342-374
- [17] Kim, K. H., Kim, C., Kim, O., E., “Methods for the Accurate Computations of Hypersonic Flows,” *Journal of Computational Physics*, Vol. 174, No.1 Nov 2001, pp. 38-80
- [18] Anderson, J. D., “Fundamentals of Aerodynamics,” 5th ed., McGraw-Hill, New York, 2011
- [19] Hoffmann, K. A., Chiang, S. T., “Computational Fluid Dynamics,” 4th ed., Engineering Education System, Kansas, 2000
- [20] Toro, E. F., “Riemann Solvers and Numerical Methods for Fluid Dynamics,” 3rd ed., Springer, Berlin, 2009
- [21] Leveque, R. J., “Finite Volume Methods for Hyperbolic Problems,” 1st ed, Cambridge University Press, Cambridge, 2002
- [22] Golub, G. H., Van Loan, C. F., “Matrix Computations,” 4th ed, The Johns Hopkins University Press, Baltimore, 2013

국문초록

본 연구는 최소제곱법 방법간의 스위칭 함수의 설계를 통해 비정렬 격자에서 정확하고 효율적인 구배 계산 제안한다. 다양한 예제들을 분석한 결과, 비정렬 격자에서 가장 널리 사용되는 구배 계산방법 중 하나인 그린-가우스 정리를 이용한 구배 계산방법이 본질적으로 inconsistent하며, 또한 최소 제곱법을 활용하는 구배 계산방법이 점성경계층 및 일반 격자에서 그린-가우스 정리를 사용하는 방법보다 더 정확함을 보였다.

앞선 분석을 바탕으로 상대적으로 효율적인 좁은 스텐실을 사용하는 가중 최소제곱법 방법과 상대적으로 정확한 넓은 스텐실을 사용하는 가중 최소제곱법 사이의 스위칭을 추구하였다. 한편 최소제곱법 행렬의 조건수가 구배 오차와 상관관계를 보이며, 오직 격자의 정보만으로도 계산이 가능하므로 이를 스위칭 기준으로 삼았다. 일반적인 격자에 적용하기 위해서 조건수를 분석한 결과, 삼각함수를 이용하여 조건수를 스텐실 개수와 스텐실 벡터간의 각도의 함수로 표현하였다. 그리고 넓은 스텐실을 사용하는 최소제곱법 방법의 평균 조건수가 적합한 스위칭 기준 값을 확인하였다.

2차원 및 3차원 간단한 문제들에 대하여 스위칭 메커니즘을 보였다. 마지막으로 SWLSQ의 우수함을 보이기 위해 2차원 익형, 3차원 윙바디 및

전투기 형상에 대해 3가지 최소제곱법 방법들의 구배 정확도와 계산 비용을 비교하였다.

주요어: 구배, 구배 계산방법, 최소제곱법, 스위칭 함수, 조건수, 그린-가우스 정리, 비정렬 격자

학번: 2017-29318